Journal Pre-proof

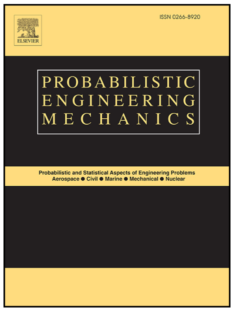

Numerical Investigation of Turbulence Effect on Flight Trajectory of Spherical Windborne Debris: A Multi-Layered Approach

Shaopeng Li, Kurtis Gurley, Yanlin Guo, John van de Lindt

PII: S0266-8920(24)00083-3

DOI: https://doi.org/10.1016/j.probengmech.2024.103661

Reference: PREM 103661

To appear in: *Probabilistic Engineering Mechanics*

Received Date: 28 March 2024

Revised Date: 14 June 2024

Accepted Date: 25 June 2024

Please cite this article as: S. Li, K. Gurley, Y. Guo, J. van de Lindt, Numerical Investigation of Turbulence Effect on Flight Trajectory of Spherical Windborne Debris: A Multi-Layered Approach, *Probabilistic Engineering Mechanics*, https://doi.org/10.1016/j.probengmech.2024.103661.

Numerical Investigation of Turbulence Effect on Flight Trajectory of Spherical Windborne Debris: A Multi-Layered Approach

Shaopeng Li[1*], Kurtis Gurley[2], Yanlin Guo[3], and John van de Lindt[4]

[1]Postdoctoral Associate, Department of Civil and Coastal Engineering,
University of Florida, Gainesville, United States
[2]Professor, Department of Civil and Coastal Engineering,
University of Florida, Gainesville, United States
[3]Assistant Professor, Department of Civil and Environmental Engineering,
Colorado State University, Fort Collins, United States
[4] Professor, Department of Civil and Environmental Engineering,
Colorado State University, Fort Collins, United States
[*]Corresponding author, shaopengli@ufl.edu

ABSTRACT: Accurate modeling of the turbulent wind field is a crucial component of risk analysis for structures to windborne debris damage. Existing studies typically simplify the complexities of wind turbulence, and the potential influence on the accuracy of debris flight modeling has not been systematically demonstrated. This study takes a multi-layered approach to numerically simulate the flight trajectory of spherical debris in a turbulent wind field. Complexities are incrementally added to the simulated wind field to systematically investigate the influence of spatial correlation and non-Gaussian features of turbulence on debris flight behavior. The sensitivity of debris flight behavior to turbulent wind features will inform the design of debris flight tracking wind tunnel tests and building façade debris vulnerability modeling efforts.

KEYWORDS: wind turbulence; spatial correlation; non-Gaussian turbulence; windborne debris; flight trajectory; numerical simulation

1 INTRODUCTION

Windborne debris poses a threat to building envelopes ranging from low-rise residential housing to tall buildings in an urban setting with glass facades/cladding systems (Minor, 1994; Gurley and Masters, 2011; Jain, 2015). Building envelope damage can lead to subsequent water intrusion, extensive interior damage, and additional debris further damaging the structure and potentially resulting in a risk to occupant safety (Pita et al., 2016; Johnson et al., 2018; Wei et al., 2024a). The resulting loss of building functionality (occupant dislocation and business interruption/closures) may last for extended periods, and hence compromise community resilience (Wei et al., 2024b), underscoring the importance of reducing the vulnerability of infrastructure to windborne debris.

The damage risk for building envelopes due to windborne debris depends on the debris type, flight initiation (e.g., Kordi and Kopp, 2011; Kakimpa et al., 2011), flight trajectory (e.g., Holmes, 2004; Baker, 2007), and impact mechanism (e.g., Fernandez et al., 2010; Masters et al., 2010; Zhang et al., 2013). Among these factors that determine the risk of building envelopes, debris flight initiation and trajectory are sensitive to turbulent wind field. Hence, accurate modeling of debris impact risk depends on an accurate understanding of the turbulent wind field around buildings. The local wind field in the rooftop region significantly affects initial conditions of debris flight, while the turbulent wake wind field directly influences debris flight trajectory and contributes to uncertainties in final debris impact/landing location and momentum. Existing studies have taken the route of simplifying approaches to model this process. For example, initial location and velocity are either arbitrarily assumed as random variables (Ai et al., 2023; Lyu et al., 2023) or based on simple parametric models on roof top flows (Dong et al., 2023). For the wake flow, only the temporally constant mean wind field based on Reynolds-averaged Navier–Stokes equations (RANS) simulation (Ai et al., 2023; Lyu et al., 2023) and spatially fully correlated wind fluctuations (Dong et al., 2023) are considered in the existing numerical studies of debris flight simulation. The simplifications in existing studies may not fully capture complex debris flight behavior in the spatiotemporally varying turbulent wake flow. Since these simplifications encompass multiple aspects of the flow, the relative influence of individual simplifications on simulation accuracy is not revealed.

A recent review of windborne debris simulation studies (Zhao et al., 2021) reveals the common use of simple unobstructed open terrain flow conditions without considering the influence of surrounding buildings on the wind field (i.e., open flow conditions). Several studies have investigated flight behavior in the mean wind field without fluctuations (e.g., Lin et al., 2006; Holmes et al., 2006), but fewer studies have incorporated the effects of turbulence. Holmes (2004) and Baker (2007) briefly discussed the effects of turbulence on the flight trajectory of compact and sheet debris. They found that turbulence can produce significant variability in individual trajectories but may have little effect on average trajectories. Karimpour and Kaye (2012) studied the stochastic nature of windborne debris, where the effects of vertical and along-wind wind fluctuations on flight distance and impact kinetic energy were investigated with a uniform two-dimensional background flow. With the authors noting the high computational cost of simulating wind fluctuations along the trajectories, the abovementioned studies assumed that all the spatial points undergo an identical fluctuation following a Gaussian distribution with a target spectrum.

Moghim and Caracoglia (2012a and 2012b) simulated a uniform (spatially identical) upward vertical gust with short duration and investigated its influence on the trajectory of compact debris as well as the impact risk for a proximate tall building. Moghim and Caracoglia (2014) extended this to a more complex turbulent wind field, where the Gaussian turbulence at discrete points on the “inlet boundary” are first simulated with prescribed cross-spectrum and then propagated through the field using Taylor’s frozen turbulence hypothesis to determine wind speed at the time stepping instantaneous location of debris in flight. Some of these numerical simulations have been validated in the wind tunnel tests (Karimpour and Kaye, 2012; Moghim et al., 2015).

In addition to straight-line wind fields, existing studies have considered vortex wind fields such as tornadoes. Noting the simplifications from neglected turbulence in many existing studies (e.g., Baker and Sterling, 2017; Abdelhady et al., 2021), computational fluid dynamics (CFD) based on large eddy simulation (LES) has been used to include the tornado turbulence in debris flight computation (e.g., Maruyama, 2011; Huo et al., 2020; Liu et al., 2021a; Liu et al., 2021b). In addition, Liu et al. (2021c) compared four different modeling schemes of tornado turbulence for debris flight analysis: (1) using mean wind velocity only, (2) using the turbulence intensity to correct the aerodynamic load determined by the mean wind velocity, (3) assuming wind fluctuations experienced by the debris follow a sinusoidal wave and (4) assuming wind fluctuations experienced by the debris follow a Gaussian distribution.

The above literature review shows that existing studies simplify the complexities of wind turbulence, such as spatial correlation and non-Gaussian features, even for open flow conditions (unobstructed boundary layer flow). The potential effects of these simplifications on the accuracy and uncertainty of debris flight modeling have not been systematically quantified. The current lack of fundamental validation and uncertainty quantification of the existing simplified debris flight modeling in less complex open flow environments hinders the confident application of debris flight simulation to more realistic urban wind conditions.

To address the knowledge gap, this study numerically simulates the flight trajectory of spherical debris traveling in an unobstructed open flow turbulent boundary layer wind field. The influence of vertical and along-wind spatial correlations and non-Gaussian features in the wind fluctuations are investigated in isolation and in combination. The sensitivity of debris flight behavior to these wind features will inform the design of debris flight tracking wind tunnel tests and building façade debris vulnerability modeling efforts that address more complex urban wind fields around mid/high-rise buildings with the presence of local vortices and wake regions.

The simulation methodology of this study is schematically shown in Fig. 1. For statistical analysis of debris flight characteristics requiring input of wind speed along the debris flight trajectory, the premise is to simulate time histories of longitudinal wind speed over a fixed spatial grid forming a vertical plane parallel to the horizontal mean wind direction. With the simulated wind field, the two-dimensional debris flight trajectories are computed by releasing N_{DR} debris at random time steps. This debris releasing process is repeated N_{WG} times, resulting in a total of $N_{DR} \times N_{WG}$ simulated debris flight trajectories for a reliable statistical estimate of the debris flight characteristics. The selection of proper values of N_{DR} and N_{WG} is discussed later in this paper.

The next two sections describe the debris flight model employed in this study and the stochastic wind field simulation approach to incorporate increasingly realistic spatial correlation features concurrent with Gaussian and then non-Gaussian probability content. The result analysis and implications for wind tunnel testing are subsequent, followed by the concluding remarks and future directions.

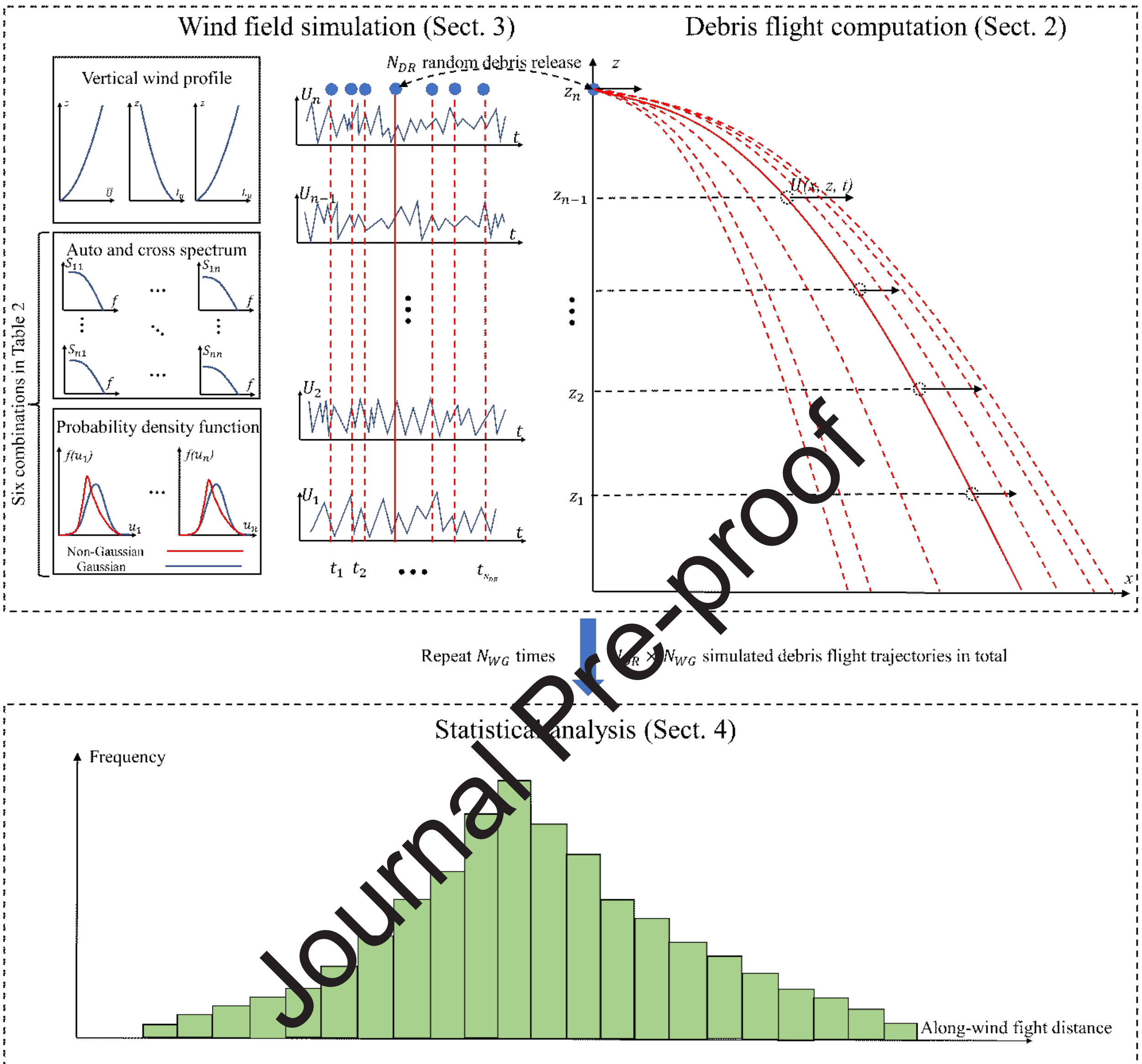

Figure 1. Schematic of the simulation methodology

2 DEBRIS FLIGHT MODEL

This study considers two-dimensional flight trajectory of spherical debris. The adoption of spherical debris allows for elimination of complex uncertainties from the time-varying aerodynamic lift/drag as in debris of irregular shapes. The two-dimensional simplification of the debris flight is justified by the open flow environment investigated in this study. The governing equation of the debris flight (see Fig. 2), based on the quasi-steady aerodynamic load, can be expressed as (Holmes, 2004):

$$m\frac{\mathrm{d}^2x}{\mathrm{d}t^2}=\frac{1}{2}\rho_a A C_d\cos\alpha\left[(U-\frac{\mathrm{d}x}{\mathrm{d}t})^2+(W-\frac{\mathrm{d}z}{\mathrm{d}t})^2\right] \quad \text{(1a)}$$

$$m\frac{\mathrm{d}^2z}{\mathrm{d}t^2}=\frac{1}{2}\rho_a A C_d\cos\gamma\left[(U-\frac{\mathrm{d}x}{\mathrm{d}t})^2+(W-\frac{\mathrm{d}z}{\mathrm{d}t})^2\right]-mg \quad \text{(1b)}$$

where x and z are the displacements in along-wind and vertical directions; t is the time; m is the mass of the debris calculated as $m=\frac{4}{3}\pi r^3\rho$ (r is the debris radius and ρ is the debris density); g is the gravitational acceleration; ρ_a is the density of air; A is the projected frontal area for a spherical debris $A=\pi r^2$; C_d is the drag coefficient; the values of these parameters are listed in Table 1, and some of them are determined by the practical considerations for the planned wind tunnel tests where the flight trajectories of scaled debris will be tracked using high-speed cameras; U and W are the wind velocity along the debris flight trajectory, varying both spatially and temporally [i.e., $U=U(x,z,t)$ and $W=W(x,z,t)$]; The trigonometric functions of angles between the relative wind speed and the two axis, denoted as α and γ, can be calculated as $\cos\alpha=\frac{U-\frac{\mathrm{d}x}{\mathrm{d}t}}{\sqrt{(U-\frac{\mathrm{d}x}{\mathrm{d}t})^2+(W-\frac{\mathrm{d}z}{\mathrm{d}t})^2}}$ and $\cos\gamma=\frac{W-\frac{\mathrm{d}z}{\mathrm{d}t}}{\sqrt{(U-\frac{\mathrm{d}x}{\mathrm{d}t})^2+(W-\frac{\mathrm{d}z}{\mathrm{d}t})^2}}$, which can be substituted into Eq. (1) to derive:

$$m\frac{\mathrm{d}^2x}{\mathrm{d}t^2}=\frac{1}{2}\rho_a A C_d(U-\frac{\mathrm{d}x}{\mathrm{d}t})\sqrt{(U-\frac{\mathrm{d}x}{\mathrm{d}t})^2+(W-\frac{\mathrm{d}z}{\mathrm{d}t})^2} \quad \text{(2a)}$$

$$m\frac{\mathrm{d}^2z}{\mathrm{d}t^2}=\frac{1}{2}\rho_a A C_d(W-\frac{\mathrm{d}z}{\mathrm{d}t})\sqrt{(U-\frac{\mathrm{d}x}{\mathrm{d}t})^2+(W-\frac{\mathrm{d}z}{\mathrm{d}t})^2}-mg \quad \text{(2b)}$$

Journal Pre-proof

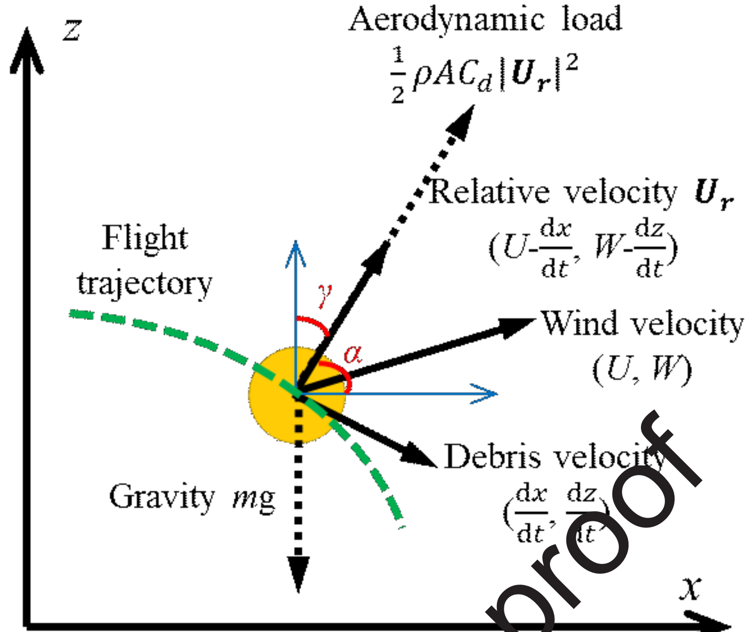

Figure 2. Schematic of simulating compact-type debris flight trajectory

Table 1. Parameters for simulating debris flight trajectories

Parameters	Values
Debris radius r	1.5 cm
Debris density ρ	2.5 g/cm^3
Debris mass m	35.3 g
Debris release height	20 m
Wind speed at release height	32.2 m/s
Drag coefficient C_d	0.5
Gravitational acceleration g	9.8 m/s^2
Air density ρ_a	1.225 kg/m^3

3 SIMULATION OF TURBULENT WIND FIELD

This section discusses the simulation of the turbulent wind field as the input to the debris flight model. Multiple schemes are employed to model the degree of correlation in the along-wind turbulence component among the spatially separated grid points, as well as the probabilistic turbulence properties. Table 2 describes the content and sequencing of six different combinations of spatial correlation and probabilistic turbulence properties used in this study, together with their implementation in debris flight model (more details in the subsections of each wind field model). To systematically analyze the influence of the spatial correlation of turbulence, Section 3.1 begins with the two extremes of no correlation and full spatial correlation to establish debris flight behavior boundaries (here the "full correlation" does not have a time delay). Considering that the key factor is the fluctuation correlation between the points along the debris flight trajectory (with coordinate variation in both vertical and along-wind direction), the cases of "no vertical and full along-wind correlation" and "full vertical and no along-wind correlation" are equivalent to the case of "no vertical and no along-wind correlation", and hence are not included in Table 2. After the two extreme cases, more realistic scenarios of partial vertical correlation and frozen turbulence-based along-wind propagation (i.e., full correlation with time delay) are investigated. Wind fluctuations in Section 3.1 are assumed to follow the Gaussian distribution, while non-Gaussian wind turbulence will be introduced later in Section 3.2.

For all simulations considered, the mean wind speed $\overline{U}(z)$ along the elevation z follows the logarithmic law (ASCE/SEI 49-12):

$$\frac{\overline{U}(z)}{U_r} = \frac{\ln[\frac{z-d}{z_0}]}{\ln[\frac{z_r-d}{z_0}]} \tag{3}$$

U_r is the reference wind speed at reference height z_r; U_r = 32.2 m/s is selected in this study with z_r = 20 m (selected based on debris releasing height for a typical mid-rise building); the debris release location is also at the reference height z_r; z_0 = 0.3 m is the roughness length for suburban terrain; d = 0.94 m is the displacement height.

The vertical profile of turbulence intensity $I_u(z)$ is modeled following (ASCE/SEI 49-12):

$$I_u(z) = \frac{1}{\ln[\frac{z-d}{z_0}]} \tag{4}$$

The wind turbulence follows the von Karman spectrum:

$$\frac{\omega S(\omega)}{2\pi\sigma_s^2} = \frac{4\left[\frac{\omega L_u(z)}{2\pi\bar{U}(z)}\right]}{\left\{1+70.8\left[\frac{\omega L_u(z)}{2\pi\bar{U}(z)}\right]\right\}^{\frac{5}{6}}} \quad (5)$$

where $\sigma_s = \bar{U}(z)I_u(z)$ is the standard deviation of the wind fluctuation; $L_u(z)$ is the turbulence integral length scale varying with elevation, which is calculated as (ASCE/SEI 7-16):

$$L_u(z) = 97.54(\frac{z}{10})^{1/3} \quad (6)$$

This study models open flow conditions (no proximity buildings) and assumes zero mean vertical wind speed, i.e., $\bar{W}$=0. Furthermore, it is expected that compared to along-wind turbulence the influence of vertical turbulence on debris flight behavior is relatively weak due to: (1) vertical turbulence intensity is usually smaller than along-wind turbulence in open flow (Hui et al., 2009; He et al., 2020), and (2) vertical turbulence usually has fewer low-frequency components in the spectrum (Dyrbye and Hansen, 1996; Moghim and Caracoglia, 2014) and hence smaller spatial scales, indicating that its effect on debris motion can be more easily canceled out during the flight. In addition, currently there is a lack a standard accepted model for the correlation between vertical and along-wind fluctuation (Benowitz and Deodatis, 2015; Liu et al., 2023). Hence, vertical turbulence is not considered in this study but will be considered in follow up work that use particle image velocimetry (PIV) measurements as the baseline wind field.

Table 2. The six combinations of spatial correlation and probabilistic turbulence properties along with their implementations in debris flight model

Section number	Correlation		Probability density function	Implementation in debris flight model
	Vertical	Along-wind		
3.1.1	None	None	Gaussian	Simulate a single Gaussian white noise-based wind fluctuation as input to debris flight model
3.1.2	Full without time delay	Full without time delay		Simulate a single Karman spectrum-based Gaussian wind fluctuation as input to debris flight model
3.1.3.1	Partial: distance-decaying	Full without time delay		Simulate multiple correlated Karman spectrum-based Gaussian wind fluctuations at different vertical locations along the inlet; use the same fluctuation for along-wind propagation; use the fluctuations at nearest locations for vertical interpolation
3.1.3.2	Partial: distance-decaying	Full with time delay: Frozen turbulence		Simulate multiple correlated Karman spectrum-based Gaussian wind fluctuations at different vertical locations along the inlet; use frozen turbulence-based time delay for along-wind propagation; use the fluctuations at nearest locations for vertical interpolation
3.2	Partial: distance-decaying	Full with time delay: Frozen turbulence	Non-Gaussian	Simulate multiple correlated Karman spectrum-based non-Gaussian wind fluctuations at different vertical locations along the inlet; use frozen turbulence-based time delay for along-wind propagation; use the fluctuations at nearest locations for vertical interpolation

3.1 Gaussian wind fluctuation with varying schemes for spatial correlation of turbulence

3.1.1 *Fluctuation with no spatial correlation*

When wind fluctuations at all spatial points on the grid are uncorrelated, the wind speed experienced by the windborne debris at any location and time $U(x,z,t)$ is simply:

$$U(x,z,t) = \overline{U}(z) + u(x,z,t) \approx \overline{U}(z) + \overline{U}(z) I_u(z) u_w(t) \quad \text{with } u_w(t) \sim N[0,1] \tag{7}$$

where $u_w(t)$ is randomly drawn from standard Gaussian white noise distribution $N[0,1]$ at each time *t*. Figure 3 illustrates the concept, where the instantaneous debris location (dashed circles) is subjected to an instantaneous speed (Eq. 7) consisting of the mean $\overline{U}(z)$ and superimposed fluctuating component (blue arrows) described by scaled white noise.

The simulated standard Gaussian white noise $u_w(t)$ is shown in Fig. 4(a), where the length of the whole simulated time series is $N_u = 2^{16}$ and time interval is $\Delta t = 0.0125$ s. The duration $T_u = 819.2$ s (resulting frequency increment $\Delta f = 0.00122$ Hz) is selected to capture sufficient low-frequency turbulence, which is also larger than the 10 min wind duration used in the literature (Karimpour and Kaye, 2012; Moghim et al., 2015). T_u is discussed further in the next section in the context of the length scale of turbulence for spatially correlated flow. The ensemble of $N_{WG} = 128$ realizations of wind fluctuations is used to obtain the spectrum in Fig. 4(b). The Δt and N_{WG}, used throughout this study, are based on the sensitivity analysis presented in Appendix A.

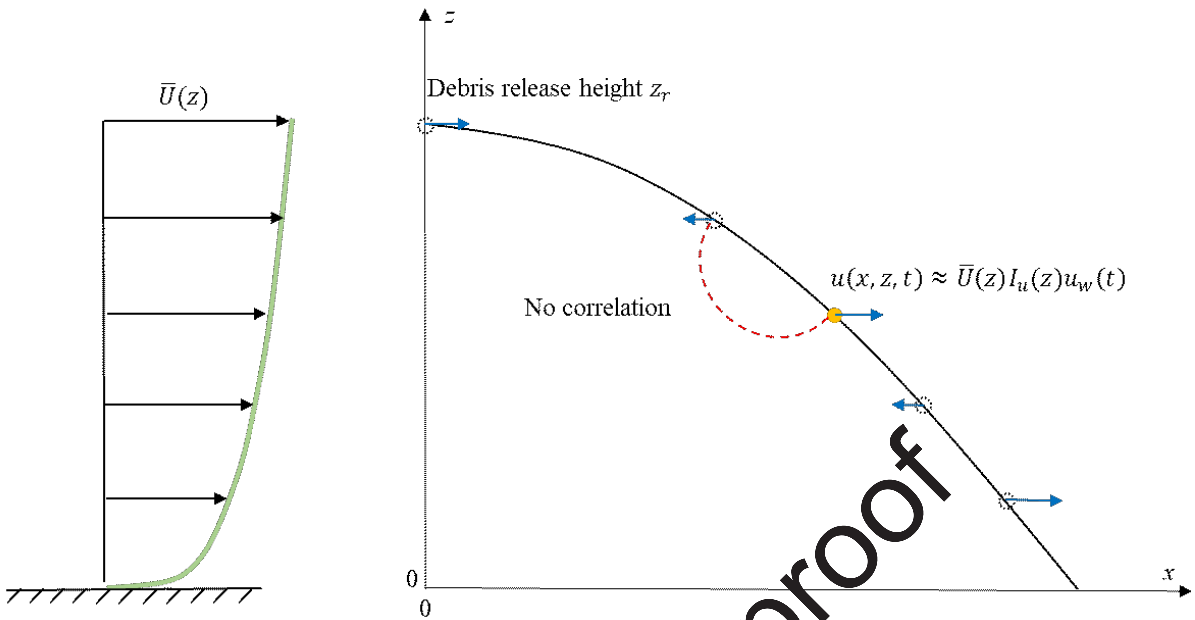

Figure 3. Wind fluctuation with no spatial correlation

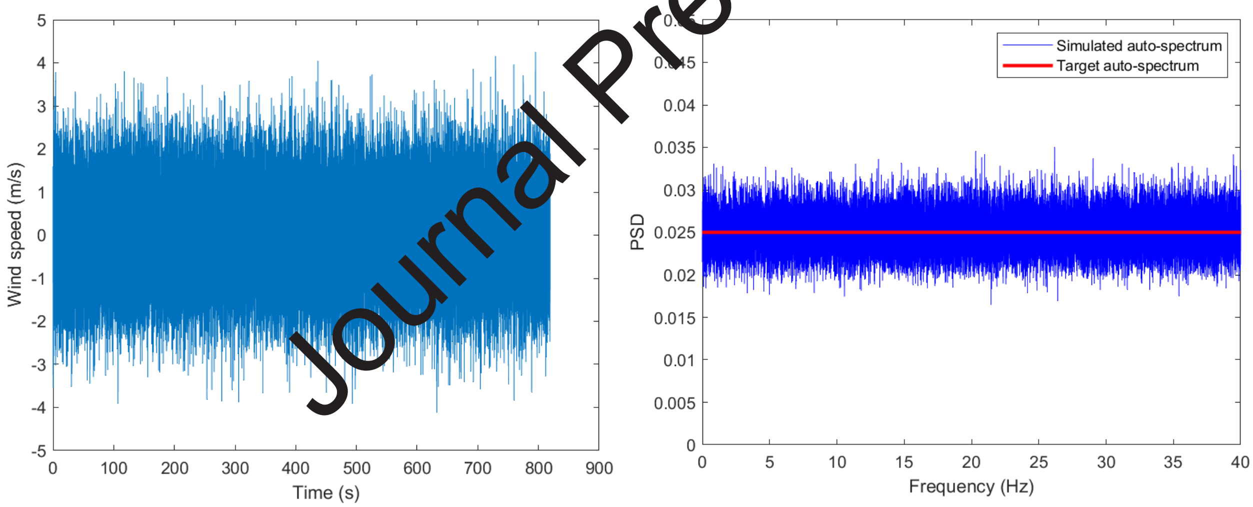

(a) Time-domain result (b) Frequency-domain result

Figure 4. No spatial correlation: simulated standard Gaussian white noise $u_w(t)$

3.1.2 *Fluctuation with full spatial correlation*

When wind fluctuations at all spatial points on the grid are fully correlated, a time history at a single grid point (say $z = z_r$ and $x = 0$) is generated. That time history is then translated and dilated to impart the appropriate mean and turbulence intensity at each height on the grid. For a given height z, the time history of wind speed at every horizontal grid point x is identical and without time lag. Under this description, the wind speed experienced by the windborne debris at any location and time $U(x, z, t)$ can be calculated as (see Fig. 5):

$$U(x, z, t) = \overline{U}(z) + u(x, z, t) \approx \overline{U}(z) + \overline{U}(z) I_u(z) u_s(t) \text{ with } F_{PSD}[u_s(t)] = S(\omega) \quad (8)$$

where $u_s(t)$ is a unit-variance wind fluctuation with prescribed power spectrum density (PSD) $S(\omega)$ based on Eq. (5). For this case, $\overline{U}(z)$ in Eq. (5) is set to be U_r while the integral length scale is $L_u(z_r)$, essentially assuming all the spatial points in the wind field undergo scaled fluctuation at reference elevation z_r (this is also the debris release location). The spectral representation method (SRM) (Deodatis, 1996) is employed to simulate the wind fluctuation $u_s(t)$ with target spectrum $S(\omega)$. A sample of simulated unit-variance wind fluctuation $u_s(t)$ is shown in Fig. 6. The wind speed simulation duration of T_u = 819.2 s was chosen to capture sufficient low frequency contribution to the wind record interacting with the debris. From Eq. 6 it was determined that at the turbulence integral length scale at the debris release height of 20 m is 122.9 m. At the employed mean wind speed of 32.2 m/s, the simulated 819.2 s record permits the sequential passage of approximately 215 integral length scales.

Through comparing Eq. (7) and Fig. 4 with Eq. (8) and Fig. 6, it is straightforward that the only difference between the no-correlation and full-correlation scenarios is the PSD of the debris-experienced fluctuation. The unit-variance wind fluctuation $u_s(t)$ has more low-frequency energy and less high-frequency energy compared to that of the standard Gaussian white noise $u_w(t)$. The difference of spectral property of $u_s(t)$ and $u_w(t)$ allows revealing the influence of turbulence frequency distribution on the debris flight, which will be discussed in the beginning of Section 4.1.

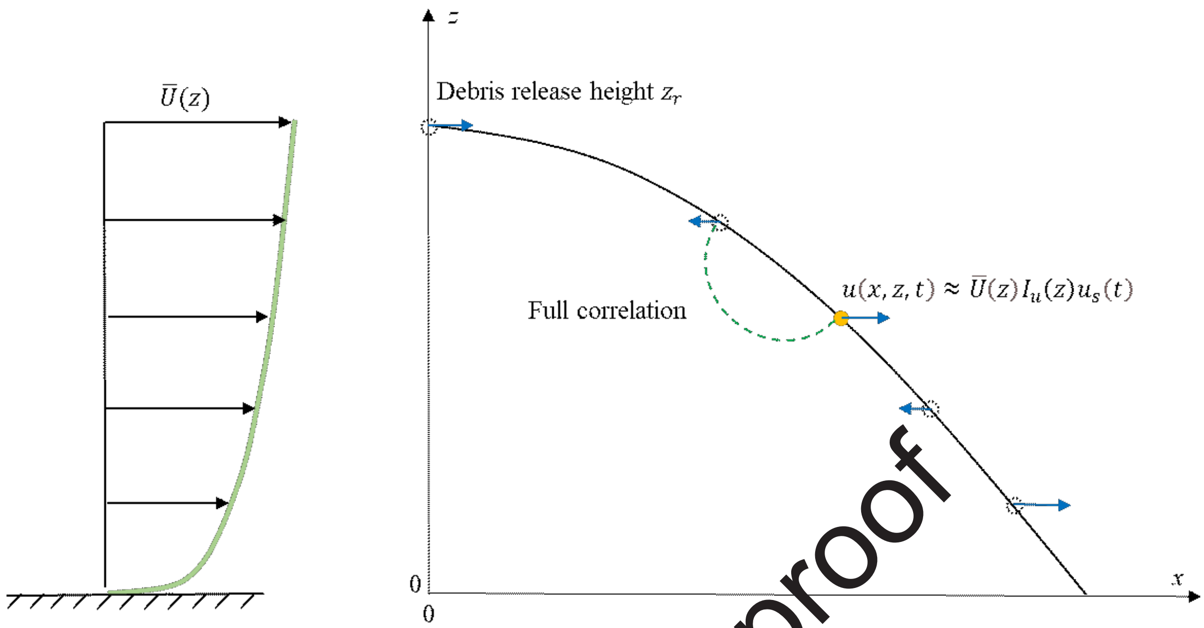

Figure 5. Wind fluctuation with full spatial correlation

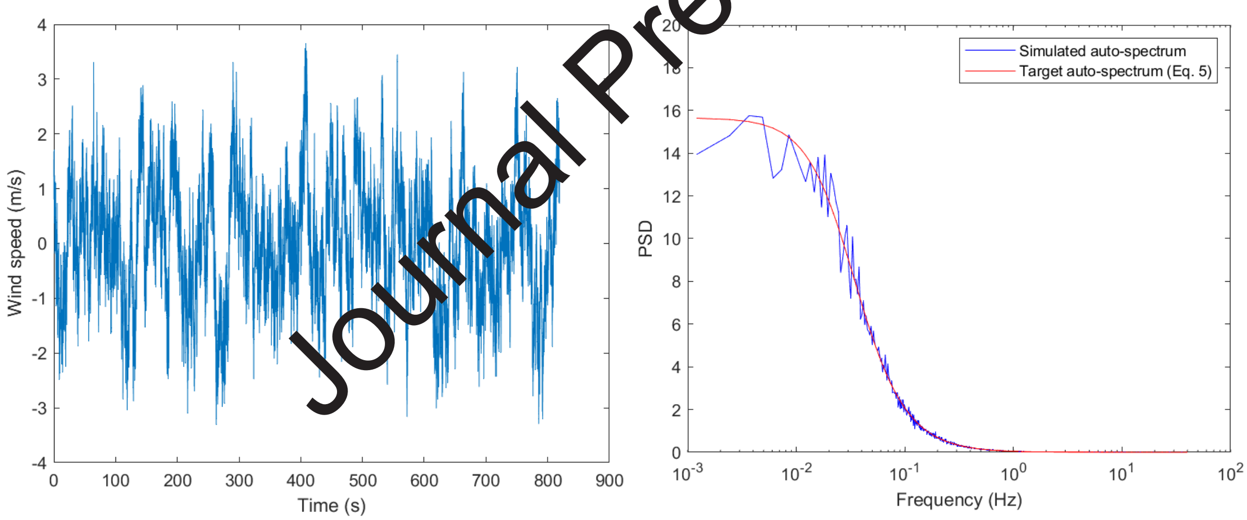

(a) Time-domain result

(b) Frequency-domain result (area under the curve is one)

Figure 6. Full spatial correlation: simulated unit-variance wind fluctuations $u_s(t)$

3.1.3 *Fluctuation with partial spatial correlation*

The upcoming results section will reveal clear differences in debris flight behaviors between the two extreme scenarios of no and full spatial correlation of turbulence, illustrating the potential importance of partial correlation on debris flight. The vertical spatial correlation of longitudinal fluctuations has been widely studied, and well-accepted models, such as Davenport's distance-decaying coherence (Davenport, 1961), are available. On the other hand, the along-wind spatial correlation of longitudinal fluctuations is less standardized. Taylor's frozen turbulence hypothesis (Taylor, 1938) is still widely presumed. In frozen turbulence-based correlation, the cross-correlation coefficient function of longitudinal turbulence between two along-wind separated locations peaks with a value of unity at the time lag determined by the distance between the two separated locations divided by the mean wind speed.

This study maintains a consistent distance-decaying partial correlation scheme in the vertical direction while considering two schemes for modeling along-wind correlation: (1) full correlation without time delay, (2) full correlation with time delay based on frozen turbulence. More realistic along-wind correlations will be considered in future work using PIV measurements as the baseline wind field.

3.1.3.1 *Distance-decaying correlation in vertical direction and full correlation in along-wind direction*

To generate wind fluctuation with partial correlation in the vertical direction and full correlation in the along-wind direction, this study first generates wind fluctuations at n discrete vertical locations along the inlet boundary from origin (0, 0) to debris release location (0, z_r) with equal spacing Δz (see Fig. 7). Then, the debris-experienced wind speed can be conveniently simulated based on the assumption of full correlation and the interpolation criteria ($z \approx k\Delta z$):

$$U(x,z,t) = \overline{U}(z) + u(x,z,t) \approx \overline{U}(z) + u(0,k\Delta z,t) = \overline{U}(z) + \overline{U}(z) I_u(z) u_k(t) \quad (9)$$

The unit-variance wind fluctuations for the n locations can be simulated by the SRM using the prescribed power spectrum density matrix (PSDM) $\boldsymbol{S}(\omega)$ (Deodatis, 1996):

$$\boldsymbol{S}(\omega) = \begin{bmatrix} S_{11}(\omega) & S_{12}(\omega) & \dots & S_{1n}(\omega) \\ S_{21}(\omega) & S_{22}(\omega) & \dots & \dots \\ \dots & \dots & \dots & \dots \\ S_{n1}(\omega) & \dots & \dots & S_{nn}(\omega) \end{bmatrix} \tag{10}$$

where the diagonal term is the auto-spectrum:

$$S_{kk}(\omega) = S_k(\omega) \text{ with } k=1, 2, \dots, n \tag{11}$$

$S_k(\omega)$ is defined by von Karman spectrum in Eq. (5); the off-diagonal term is the cross-spectrum:

$$S_{jk}(\omega) = \sqrt{S_j(\omega)\, S_k(\omega)}\,\gamma_{jk}(\omega) \text{ with } j, k=1, 2, \dots, n \text{ and } j \neq k \tag{12}$$

where $\gamma_{jk}(\omega)$ is the Davenport coherence function (Davenport, 1961) with a constant decay factor $C_z = 10$:

$$\gamma_{jk}(\omega) = \exp\left\{-\frac{\omega}{2\pi}\frac{C_z|z_i - z_k|}{\frac{1}{2}[\bar{U}(z_i)+\bar{U}(z_k)]}\right\} \tag{13}$$

Wind fluctuations are simulated at 19 locations from z = 2 m (below which log law in Eq. 3 may become invalid) to release height of 20 m, where Δz is 1 m (see the sensitivity analysis in Appendix A). A sample of the simulated partially correlated wind fluctuations at elevations 20 m and 2 m, i.e., $u_{19}(t)$ and $u_1(t)$, are shown in Fig. 8, together with their auto- and cross-spectrum.

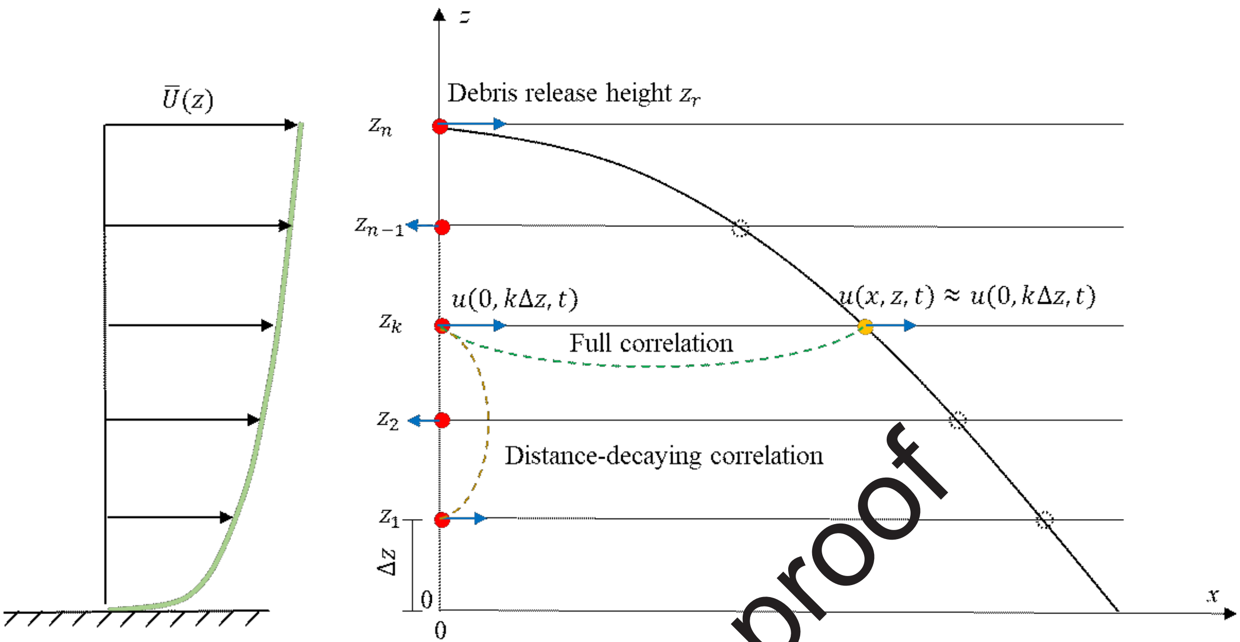

Figure 7. Wind fluctuation with partial correlation in vertical direction and full correlation in along-wind direction

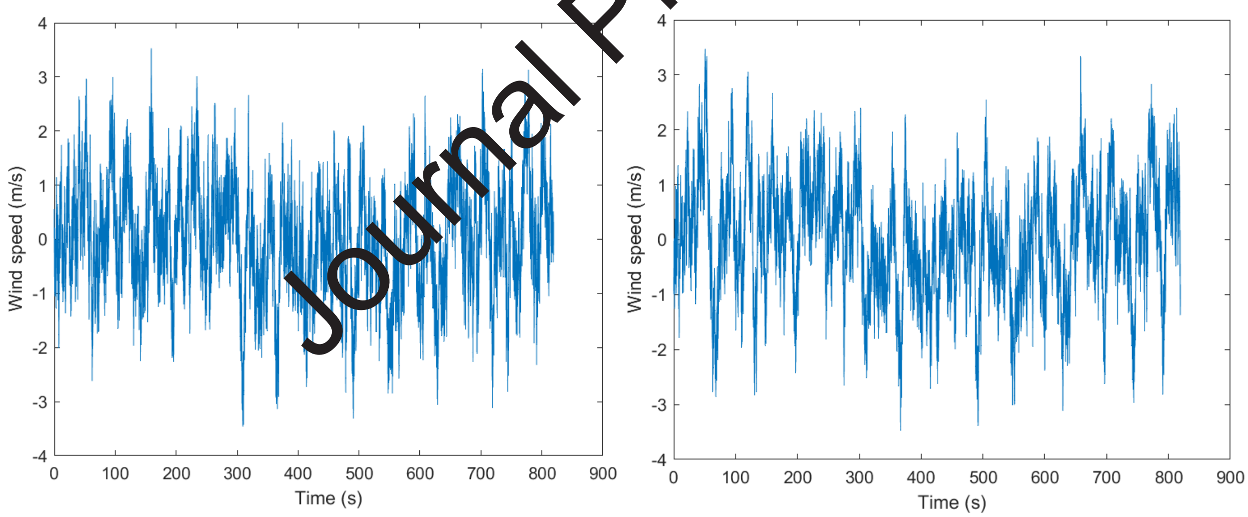

(a) Time histories of $u_{19}(t)$ (z = 20 m) (b) Time histories of $u_1(t)$ (z = 2 m)

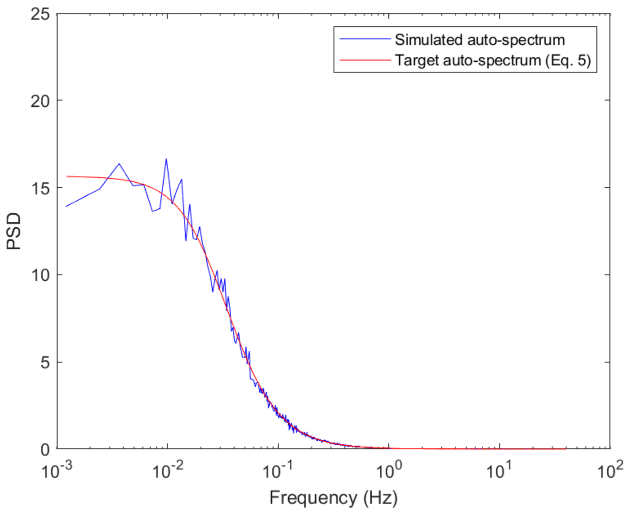

(c) Auto-spectrum of $u_{19}(t)$

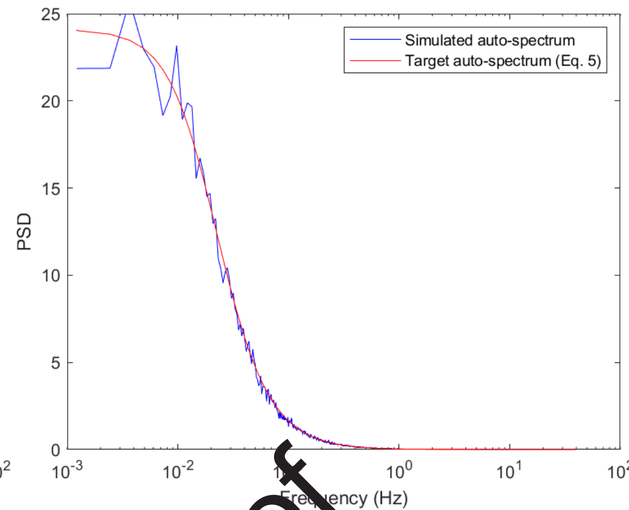

(d) Auto-spectrum of $u_1(t)$

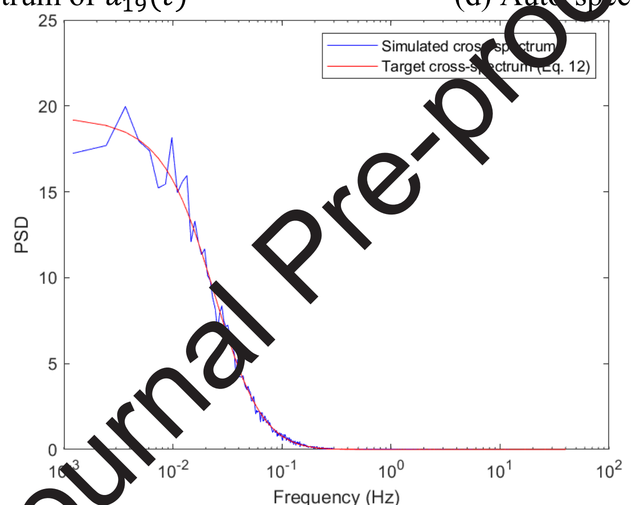

(e) Cross-spectrum of $u_{19}(t)$ and $u_1(t)$

Figure 8. Simulated correlated wind fluctuations at two elevations

3.1.3.2 *Distance-decaying correlation in vertical direction and frozen turbulence-based correlation in along-wind direction*

This section considers turbulence correlation in along-wind direction that is more realistic than full correlation. One simple approach to use Taylor's hypothesis of frozen turbulence (Taylor, 1938), which considers the downstream turbulence as the time-delayed version of upstream turbulence at the inlet boundary (see Fig. 9). Under frozen turbulence, the debris-experienced wind speed is calculated as:

$$U(x,z,t) = \bar{U}(z) + u(x,z,t) \approx \bar{U}(z) + u\left(0, k\Delta z, t - \frac{x}{\bar{U}(z)}\right)$$

$$= \bar{U}(z) + \bar{U}(z) I_u(z) u_k\left(t - \frac{x}{\bar{U}(z)}\right) \quad (14)$$

where $u_k(t)$ is the same as that defined in the previous section.

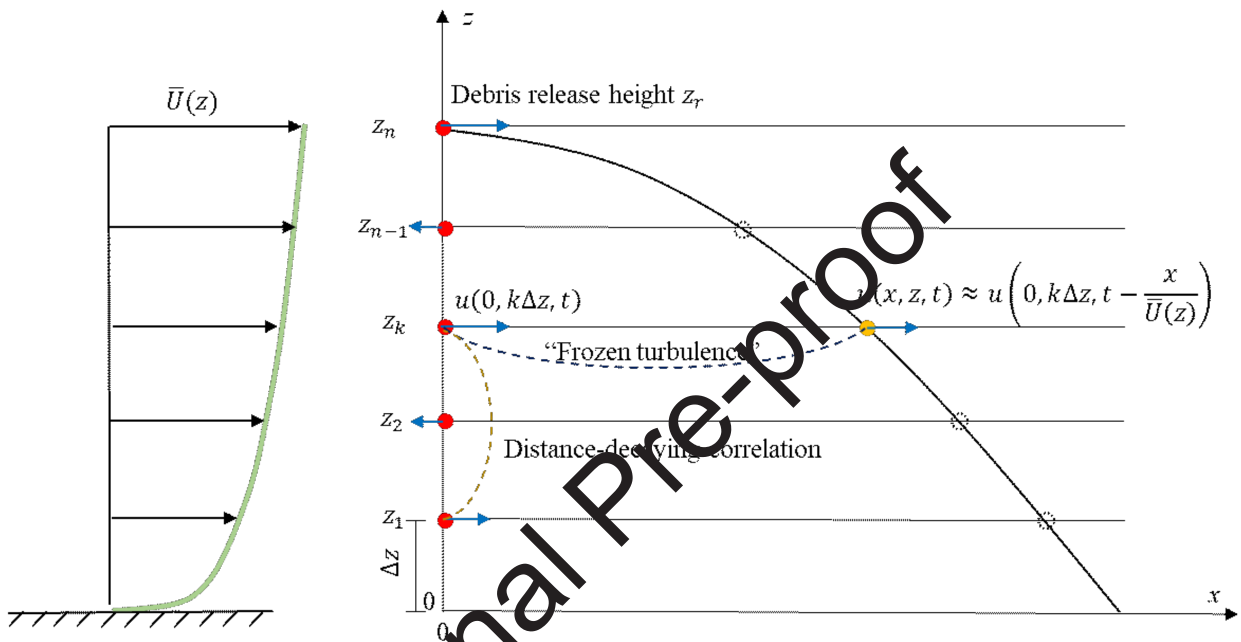

Figure 9. Wind fluctuation with partial correlation in vertical direction and frozen turbulence-based propagation in along-wind direction

3.2 Non-Gaussian wind fluctuation

The SRM simulation method employed for all correlation variations (Section 3.1) result in Gaussian wind fluctuations, which does not align with full-scale and wind tunnel observations, including extreme winds (e.g., Balderrama et al., 2012; Fernández-Cabán and Masters, 2017; Zhao et al., 2019; Gurley et al., 2021; Ojeda-Tuz et al., 2023). Non-Gaussian wind fluctuations may change the debris flight trajectory and will be investigated in this section. As described in Table 2, only the distance-decaying vertical correlation and frozen turbulence-based along-wind correlation are considered, and maintained as:

$$U(x,z,t) = \overline{U}(z) + u^N(x,z,t) \approx \overline{U}(z) + u^N\left(0, k\Delta z, t - \frac{x}{\overline{U}(z)}\right)$$

$$= \overline{U}(z) + \overline{U}(z) I_u(z) u_k^N\left(t - \frac{x}{\overline{U}(z)}\right) \quad (15)$$

The approach to simulating $u_k^N(t)$ utilizes the translation method (Grigoriu, 1984; Grigoriu, 1998) to impart the desired marginal probability density function (MPDF) and adopts a third order Hermite polynomial probability model (Yang et al., 2013; Yang and Gurley, 2015) to describe the MPDF as a function of desired skewness and kurtosis in the turbulence. In summary, the method employs a static polynomial transform of a SRM simulated Gaussian process to simultaneously achieve the desired PSD and MPDF characteristics. The approach is non-iterative and computationally efficient. Although no new contributions to this method are developed in the current study, it is briefly described in Appendix B for the sake of completeness.

Since the purpose of this section is to determine whether debris flight is sensitive to non-Gaussian turbulence features, a simple approach is employed. A uniform skewness profile with a value of $\mu^{SK}(z) = 1$ is assumed, which is relatively extreme in the context of field measurements (e.g., Balderrama et al., 2012; Fernández-Cabán and Masters, 2017; Zhao et al., 2019). The kurtosis is obtained from the empirical relationship $\mu^{KT}(z) = 2.86|\mu^{SK}(z)|^2 + 3.02 = 5.88$ from hurricane field measurement (Zhao et al., 2019). The second order characteristic follows the identical spectral and coherence models defined in the previous section. Samples of simulated non-Gaussian wind fluctuations are shown in Fig. 10, together with their skewness and kurtosis as well as the auto- and cross-spectrum.

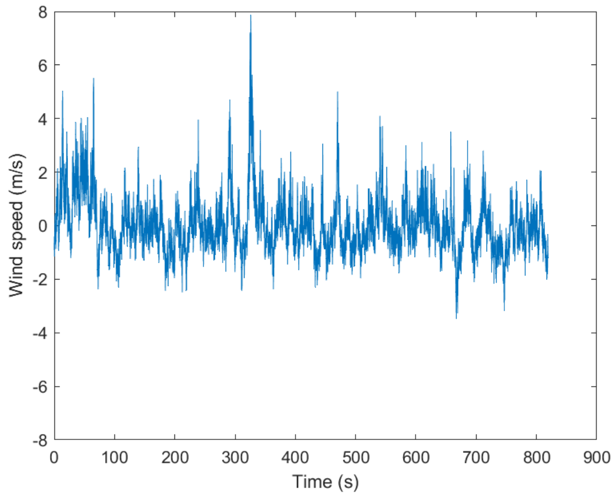

(a) Time histories of $u_{19}^{N}(t)$

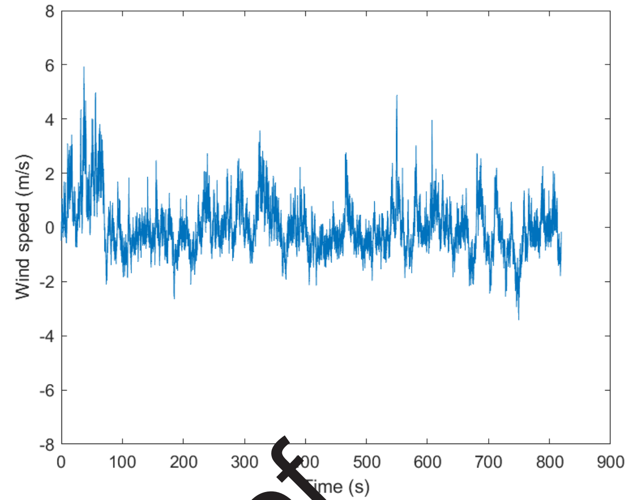

(b) Time histories of $u_{1}^{N}(t)$

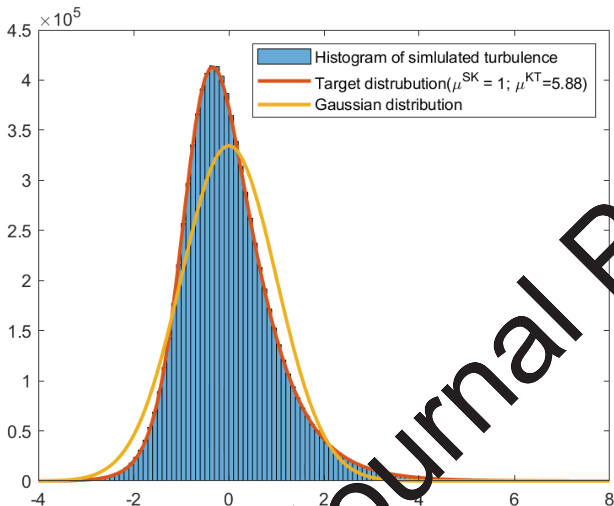

(c) Statistics of $u_{19}^{N}(t)$

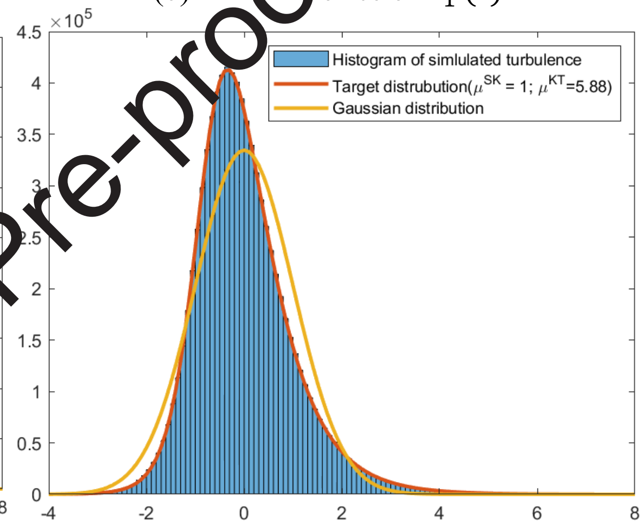

(d) Statistics of $u_{1}^{N}(t)$

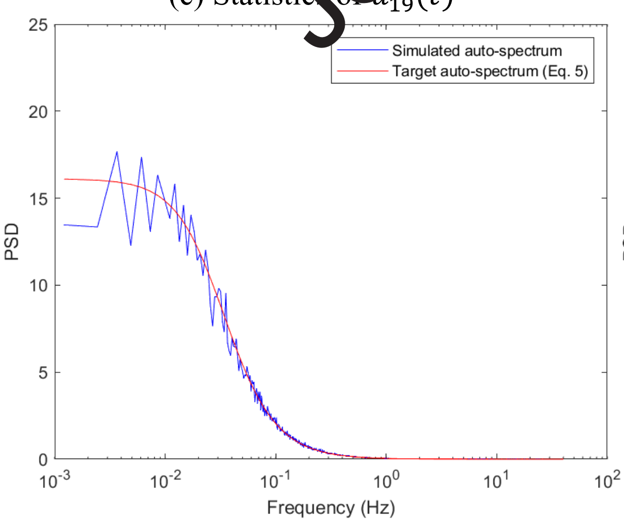

(e) Auto-spectrum of $u_{19}^{N}(t)$

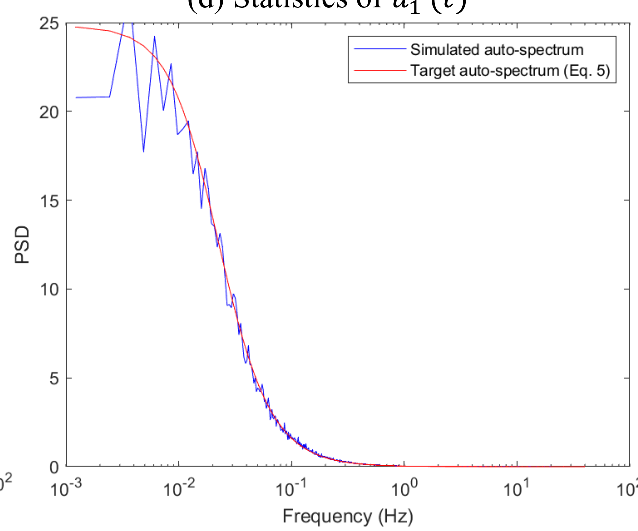

(f) Auto-spectrum of $u_{1}^{N}(t)$

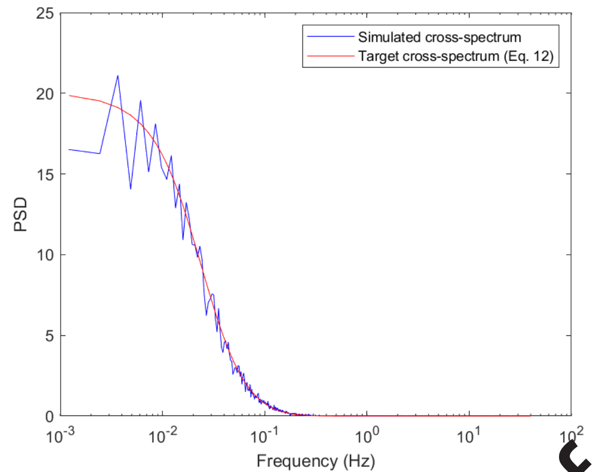

(g) Cross-spectrum of $u_{19}^N(t)$ and $u_1^N(t)$

Figure 10. Simulated non-Gaussian wind fluctuations

4 ANALYSIS OF RESULTS

The six combinations of spatial correlation and probability content (see Table 2) are employed individually to compute the flight trajectories of spherical debris using the model described in Section 2. This allows the systematic investigation of the influence of spatial correlation and the non-Gaussian probability on debris flight.

To obtain a reliable estimate on the statistical properties of simulated debris flight, the following parameters need to be properly selected for the balance of computational accuracy and efficiency: (1) the temporal discretization size, Δt, for wind field simulation and debris flight computation, (2) the spatial discretization size, Δz, for wind field simulation, (3) the number of realizations, N_{WG}, for wind field simulation, and (4) the number of debris releases, N_{DR}, for uncertainty quantification of debris flight. Sensitivity analysis is presented in Appendix A to determine appropriate values for these parameters. As a result, the values Δt = 0.0125 s, Δz = 1 m, $N_{WG} = 128$, and $N_{DR} = 2^{15}$ are adopted for this study. Zero initial velocity of debris is assumed for all scenarios. This study focuses on the statistical properties, i.e., mean, standard deviation (STD), skewness, and kurtosis, of the along-wind flight distances L_x that are important for debris risk analysis. In the following presentations, histograms of debris flight distance are presented and compared among the different experiments in Table 2. The probabilistic distribution of debris flight distance is not normalized to an empirical probability density function but kept as a histogram format to allow easier comparisons among figures.

4.1 Influence of turbulence spatial correlation on debris flight

The simulation results of the two extreme scenarios for no and full spatial correlations are shown in Fig. 11(a) and 11(b), respectively. While the mean value of flight distance is very similar, the standard deviation of the debris flight distance for the full-correlation case is almost 10 times larger than that of the no-correlation case. In addition, the distribution of along-wind flight distance is approximately Gaussian for no spatial correlation of turbulence. When full spatial correlation is introduced, the debris flight distribution becomes slightly non-Gaussian with positive skewness and kurtosis larger than 3. These results also demonstrate the influence of low-frequency fluctuations on computing debris flight, considering the differences between the flat white noise spectrum (Fig. 4b) and frequency-decaying von Karman spectrum (Fig. 6b).

It is known that an actual wind field is neither uncorrelated nor fully correlated, and so this comparison is intended to set the boundaries of correlation influence on debris flight behavior within the context of the selected conditions (release height, open flow, spherical debris, etc.). It can be concluded that the presence of correlation is a significant contributor to simulated debris flight behavior. It remains to be determined how sensitive simulated debris flight is to the layered complexities of correlation that span no-correlation through full correlation, as well as the influence of non-Gaussian turbulence.

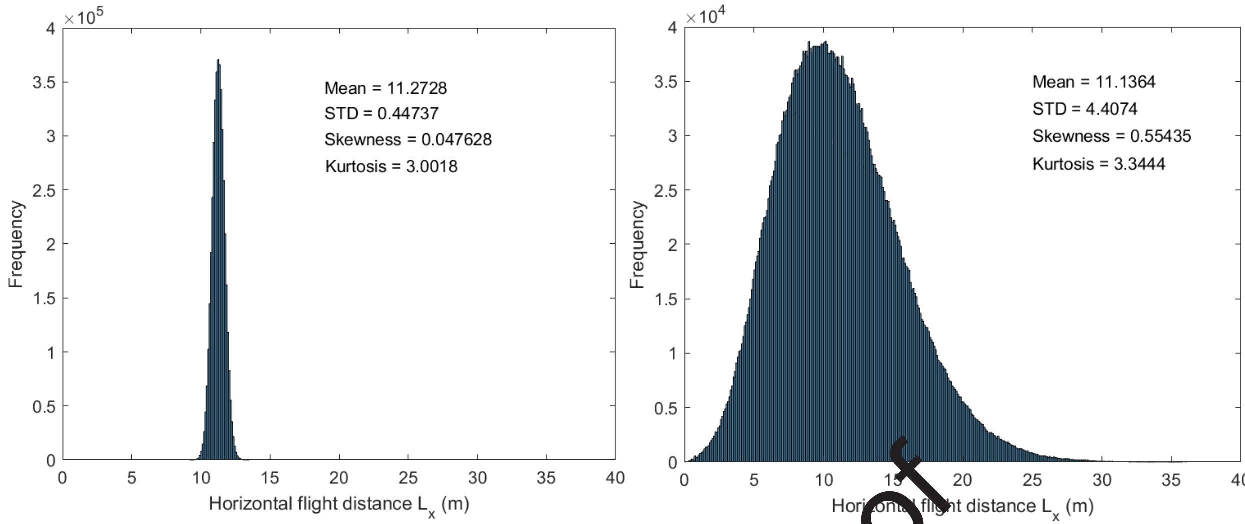

(a) Gaussian turbulence; No spatial correlation (b) Gaussian turbulence; Full spatial correlation

Figure 11. Influence of turbulence spatial correlation on debris flight

4.1.1.1 *Influence of vertical correlation*

The influence of vertical correlation is investigated through comparing the result of (1) full spatial correlation (Section 3.1.2) and (2) distance-decaying vertical correlation and full along-wind correlation (Section 3.1.3.1). The results in Fig. 12 show that the difference between the two scenarios is very small. To further investigate the underlying mechanism, two hypotheses are proposed here.

Hypothesis A: Spatial correlation is large over the relatively short distance between debris release elevation and the ground (as per the Davenport coherence function). That is, this example contrasts full vertical correlation with very large but not full vertical correlation, and little difference is observed.

Hypothesis B: Debris flight trajectories are mostly sensitive to the turbulence at the early stage of flight, and the local wind field covering the initial portion of the debris flight is highly correlated to the wind fluctuation at the debris release location.

Hypothesis A is tested by conducting simulations of debris released at 100 m elevation, where the turbulence correlation between debris release elevation and the ground is much smaller than the case of a 20 m release elevation. The simulation results (not shown) yield insignificant differences between (1) full spatial correlation and (2) distance-decaying vertical correlation and full along-wind correlation, which disproves Hypothesis A.

To test Hypothesis B, two additional cases, deviating from baseline of distance-decaying vertical correlation and full along-wind correlation, are considered: (1) no turbulence for debris traveling between z = 0 m and z =10 m, (2) no turbulence for debris traveling between z = 10m and z =20 m. The simulation results are shown in Fig. 13. For the case of no turbulence for lower portion of debris flight, the debris flight characteristics (Fig. 13c and 13d) are very close to the baseline (Fig. 13a and 13b). The debris has proved the importance of turbulence in the initial flight, which supports Hypothesis B. In contrast, the case of no turbulence for upper portion of debris flight (Fig. 13e and 13f) has significantly smaller variation in debris flight distance, which reconfirms the higher importance of turbulence in the initial stage of debris flight. This finding of higher importance of turbulence in the initial stage is also consistent with that reported in the literature (Dong et al., 2023). Additional simulations using the "temporal" half to partition the initial and later flight stage have also been conducted in Appendix C to complement the result in Fig. 13 using "spatial" half.

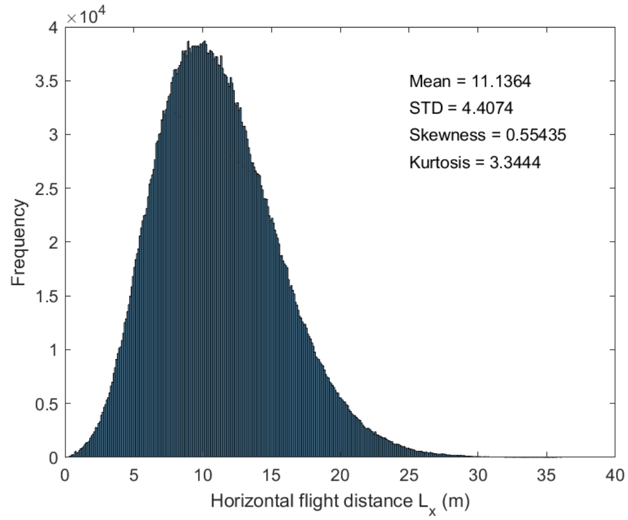

(a) Gaussian turbulence; Full spatial correlation

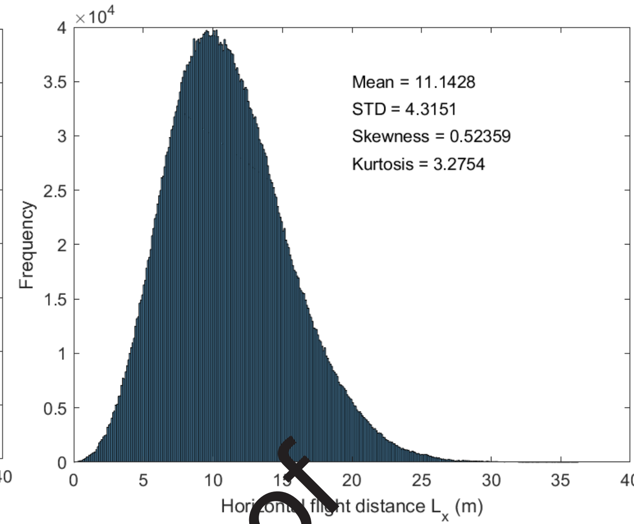

(b) Gaussian turbulence; Distance-decaying vertical correlation and full along-wind correlation

Figure 12. Influence of vertical correlation on debris flight

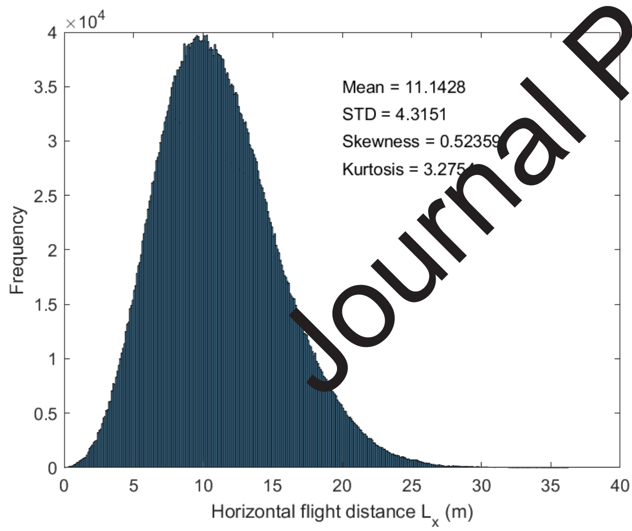

(a) Baseline: repeat of Figure 12b

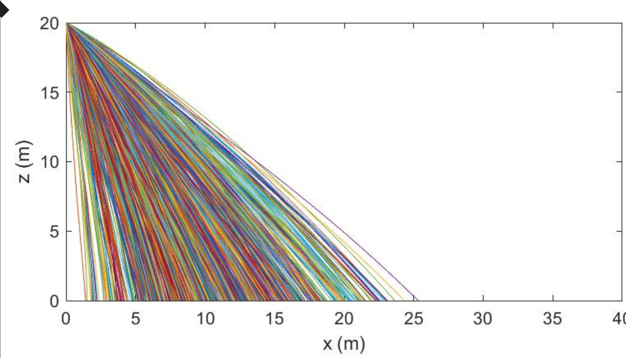

(b) 1024 samples of debris flight trajectories from Fig. 13a / 12b

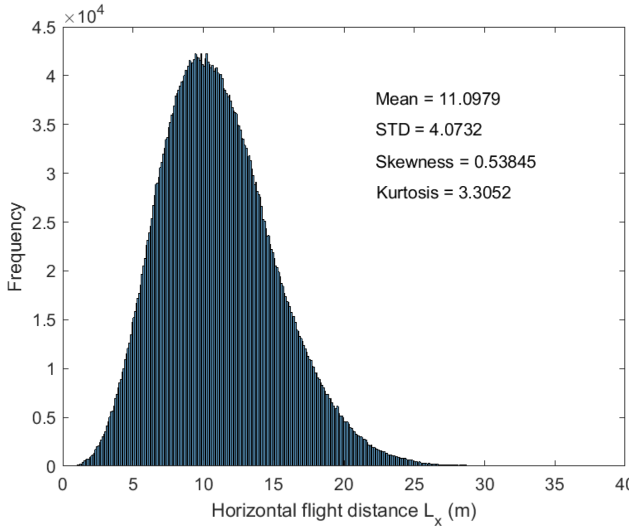

(c) Similar correlation scenario as Fig. 13a, but no turbulence for debris traveling between *z* = 0 m and *z* =10 m

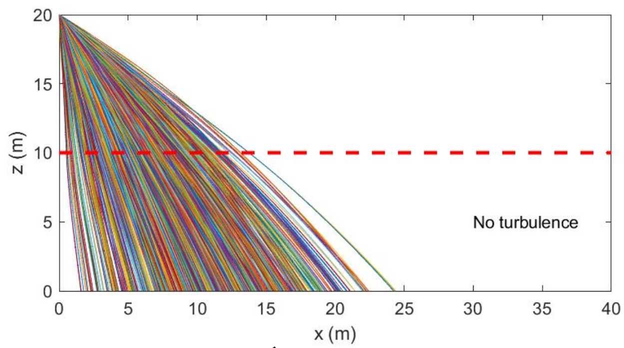

(d) 1024 samples of debris flight trajectories from Fig. 13c

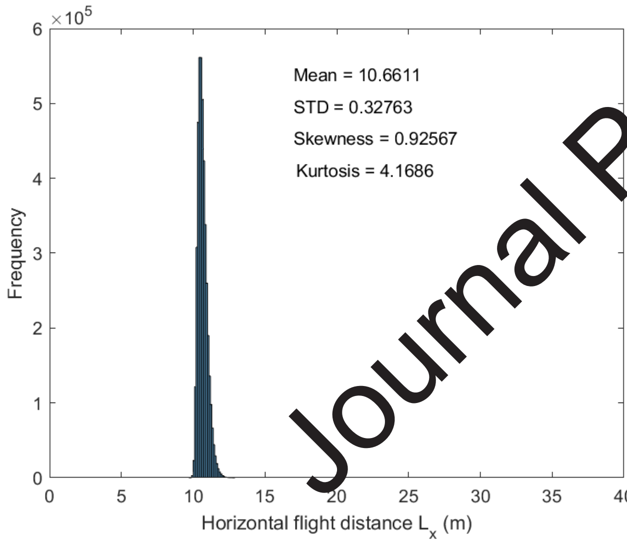

(e) Similar correlation scenario as Fig. 13a, but no turbulence for debris traveling between *z* = 10 m to *z* =20 m

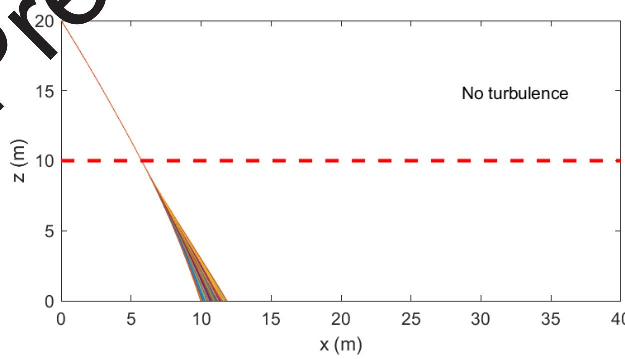

(f) 1024 samples of debris flight trajectories from Fig. 13e

Figure 13. Dissection of vertical correlation's influence on debris flight

4.1.1.2 *Influence of along-wind correlation*

The influence of along-wind correlation is investigated by comparing the result of (1) distance-decaying vertical correlation and full along-wind correlation (Section 3.1.3.1) and (2) distance-decaying vertical correlation and frozen turbulence-based along-wind correlation (Section

3.1.3.2). The results in Fig. 14 suggest very small differences between the two scenarios. This negligible difference can be attributed to the short time delay calculated in the frozen turbulence-based assumption (Eq. 14) due to the small flight distance and high wind speed. This short time delay (e.g., in the order of 0.25s for the flying debris at x = 6m and z = 10m) is smaller than the large period of low-frequency turbulence (e.g., the passage time of an integral length scale for the wind turbulence at z = 10m is in the order of 4s), and the resulting variation in wind speed is not significant for debris flight.

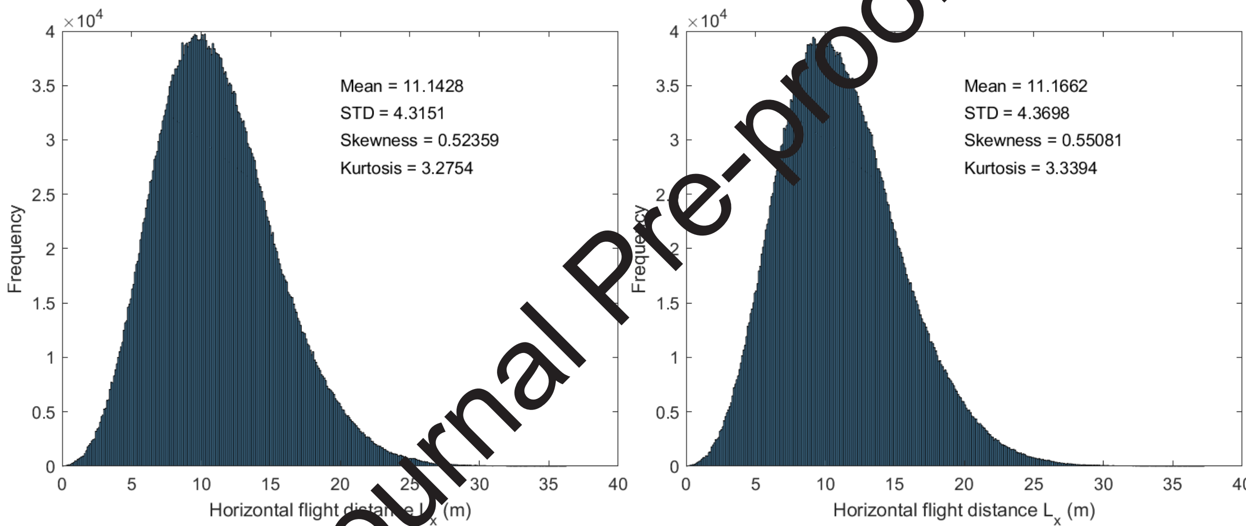

(a) Gaussian turbulence; distance-decaying vertical correlation and full along-wind correlation

(b) Gaussian turbulence; distance-decaying vertical correlation and frozen turbulence-based along-wind correlation

Figure 14. Influence of horizontal correlation on debris flight

4.2 Influence of turbulence high-order statistics on debris flight

This section investigates influence of high-order turbulence behavior on debris flight by comparing the result of Gaussian (Section 3.1.3.2) and non-Gaussian turbulence (Section 3.2) while maintaining the same spatial correlation and power spectral characteristics in both cases (distance-decaying vertical correlation and frozen turbulence-based along-wind correlation). Fig. 15a and 15b shows that the mean value of the horizontal flight distance remains unchanged, while the standard deviation slightly increases due to the non-Gaussian turbulence. The most pronounced difference is that the skewness and kurtosis of debris flight distance are much larger compared to the Gaussian counterparts. The probability of exceedance $p(L_x > \mu^{MN} + n\mu^{SD})$ for debris flying beyond n times the standard deviation, μ^{SD}, from the mean value, μ^{MN}, is shown in Fig. 15c, which shows that a Gaussian simulation underestimates the debris flight distance for the extreme cases (the tail region beyond two standard deviation away from mean). These results demonstrate the potential importance of considering non-Gaussian wind fields in debris risk analysis.

For the sake of clarity, the simulation results of all the investigated scenarios are summarized in Fig. 16.

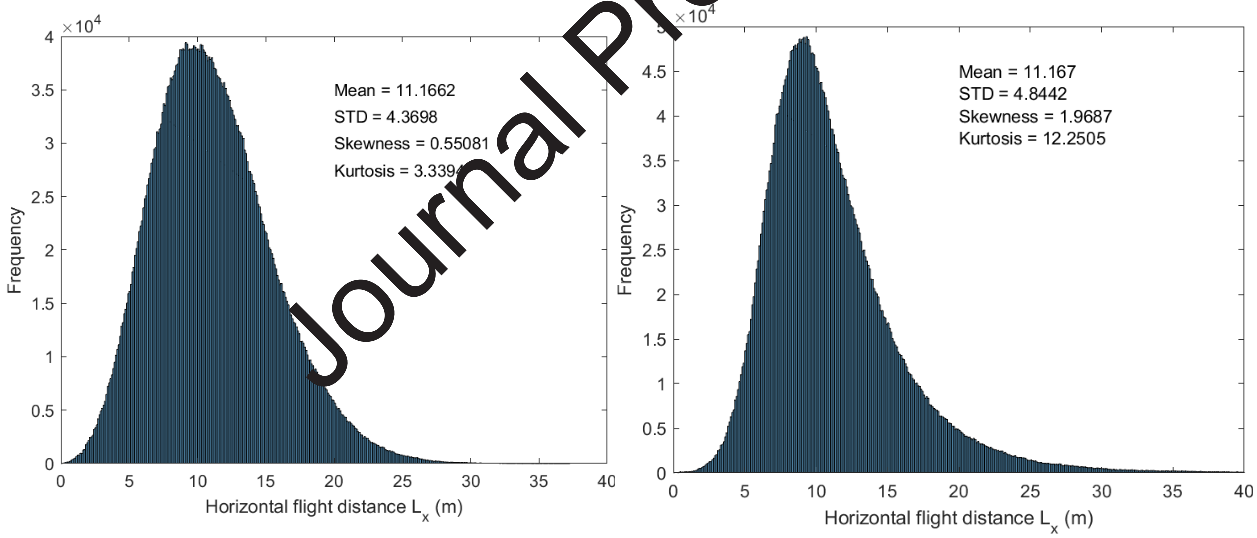

(a) Gaussian turbulence; distance-decaying vertical correlation and frozen turbulence-based along-wind correlation

(b) Non-Gaussian turbulence; distance-decaying vertical correlation and frozen turbulence-based along-wind correlation

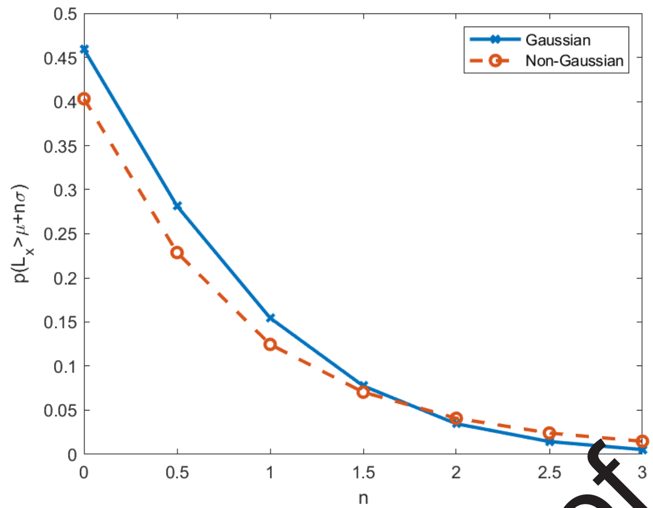

(c) Influence on probability of exceedance

Figure 15. Influence of turbulence high-order statistics on debris flight

431

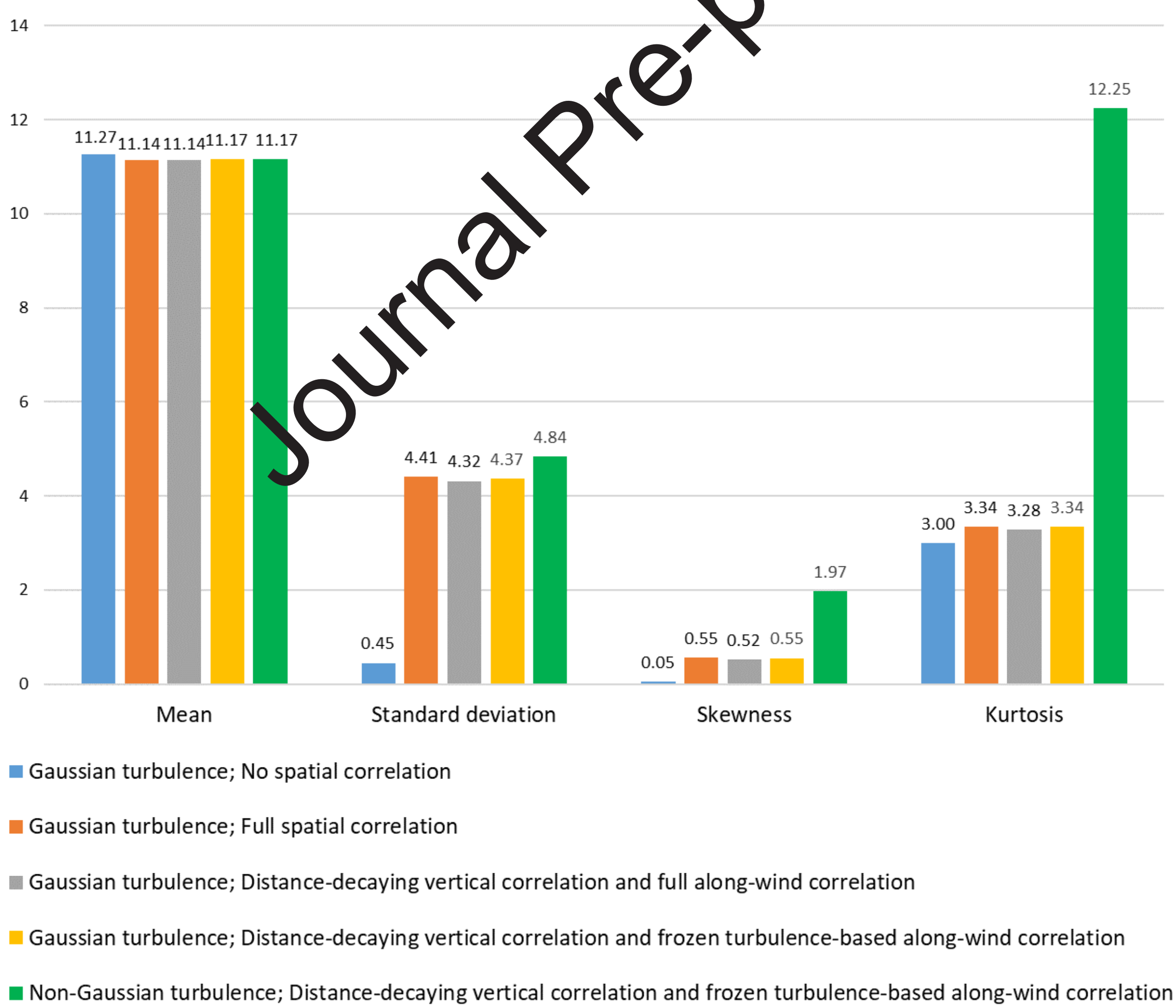

432

433 **Figure 16**. Summary of simulation results

5 IMPLICATIONS FOR WIND TUNEL TESTING

Noting that the debris shape, size and density, release height, wind speed and spectral model used in this study are selected to emulate the conditions feasible in a boundary layer wind tunnel, the obtained results can effectively inform decisions regarding experimental studies of tracking spherical debris flight. The main implications for wind tunnel testing are summarized in the following.

(1) The significant influence of low-frequency turbulence on debris flight demonstrates the value of introducing active turbulence generation such as active controlled fans (e.g., Catarelli et al., 2020; Li et al., 2021) to address the low-frequency turbulence deficit in conventional wind tunnels that employ only passive turbulence generation mechanisms.

(2) Considering the limited number of debris flight tracking tests in the wind tunnel, debris should be sequentially released to the turbulent flow with a relatively large interval so that enough number of low-frequency turbulence can be covered (i.e., avoid the case that all debris are trapped in one single gust).

(3) Based on the statistics of the debris horizontal flight distance, L_x, the view window of the debris tracking system (e.g., high-speed cameras) under the wind speed considered in this study should cover twice the distance of the debris release elevation in the along-wind direction so that the extreme values of debris landing locations can be captured.

(4) Noting the higher importance of turbulence in the initial region of debris flight, it is critical to deploy more velocity probes and/or PIV measurements near the debris release location for the future validation of numerical debris flight model against experimental results.

6 CONCLUDING REMARKS AND FUTURE DIRECTIONS

This study systematically investigates the influence of spatial correlation and high-order statistics of wind field turbulence on the flight of spherical windborne debris via numerical stochastic simulations of the wind field and debris flight. The results show that capturing partial vertical correlation and the application of Taylor's frozen turbulence in the horizontal produce results similar but not identical to the simplifying assumption of full correlation. Proper modeling of spatial correlation during the initial stages of the flight was far more critical than the modeling of turbulence after sufficient debris momentum was achieved. When spatial correlation is non-zero, Gaussian wind fluctuations produced slightly non-Gaussian distribution of debris flight distance with positive skewness and kurtosis larger than 3. The non-Gaussian features of debris flight distance are amplified when using non-Gaussian turbulence statistics (skewness and kurtosis) with values informed by field measurements of extreme winds, and the extreme values of flight distance have larger occurrence probabilities compared to the Gaussian counterpart.

Future directions may include consideration of different debris type (e.g., rod or plate) and properties (e.g., size, density, and release height) in the sensitivity analysis. The uncertainties in aerodynamic drag on the debris needs to be addressed. Experimental studies involving PIV-based wind field measurement and high-speed camera-based debris tracking will be useful to validate the model of wind field and debris flight. Moving beyond the simple open flow condition to consider the interfering effects of buildings is also a critical step to conduct debris risk analysis for realistic urban wind environment. Potential challenges that need to overcome include (1) efficient and accurate simulations of urban wind environments, (2) clear understanding of debris generation mechanism, and (3) faithful characterization of aerodynamic load on debris with irregular shapes.

7 ACKNOWLEDGEMENTS

The support from NSF grant nos. 2153751 and 2153762, as well as the NSF NHERI shared use facility award no. 2037725 is gratefully acknowledged. Any opinions, findings, and conclusions or recommendations expressed in this material are those of the authors and do not necessarily reflect the views of NSF.

APPENDIX A: SENSITIVITY ANALYSIS FOR NUMERICAL ACCURACY

This Appendix conducts the sensitivity analysis regarding the effect of spatial (Δz) and temporal discretization (Δt) as well as the number of repeating wind fluctuation generation (N_{WG}) and debris release (N_{DR}) on the computed flight trajectories based on Monte Carlo simulations. The proper values of these four parameters are sequentially determined in the following fashion. First, sensitivity analysis regarding Δt is conducted based on the debris flight distance in along-wind direction L_x under only mean wind speed without turbulence. Then, the proper value of N_{WG} is determined when the ensemble of N_{WG} realizations of wind fluctuations u (using the SRM in Section 3.1.2) achieves target Gaussian statistics (i.e., skewness $\mu^{SK}(u)$ and kurtosis $\mu^{KT}(u)$ are 0 and 3 respectively). After that, N_{DR} debris is randomly released at different time steps of the simulated winds with full spatial correlation (as in Section 3.1.1 with no need for spatial discretization), where the results of interest are selected as mean μ^{MN}, standard deviation μ^{SD}, skewness μ^{SK}, and kurtosis μ^{KT} of L_x. With the selected Δt, N_{WG} and N_{DR}, the proper size of Δz is obtained using the wind fluctuations with distance-decaying vertical correlation and full along-wind correlation (Section 3.1.3.1).

The results of the sensitivity analysis are shown in Fig. A1 to A 4. Fig. A1 shows that the temporal discretization can be selected as Δt = 0.0125 s, beyond which the value of L_x stabilizes.

Fig. A2 reveals that the repeat times of wind generation can determined as N_{WG}= 128. Similarly, Fig. A3 indicate that number of debris release can be determined as $N_{DR} = 2^{15}$, while Fig. A4 suggests that the spatial discretization of Δz = 1 m to sufficient to obtain a reliable estimate of the statistics.

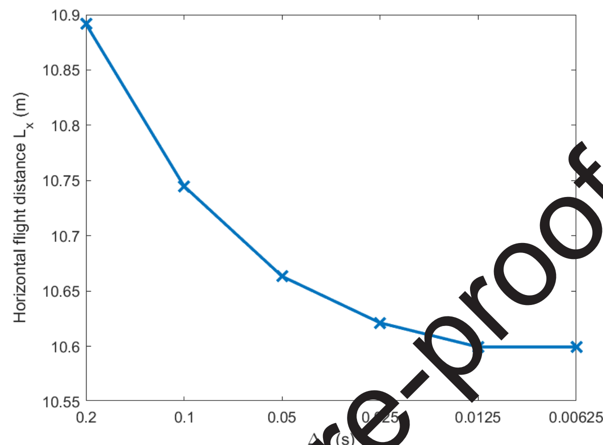

Figure A1. Sensitivity analysis on Δt

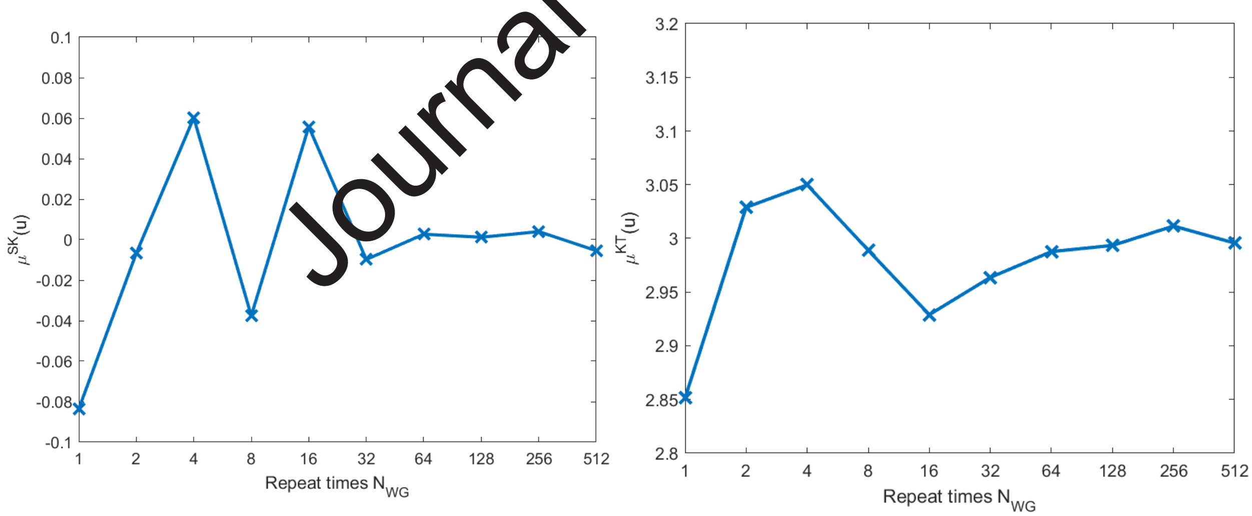

(a) Skewness (b) Kurtosis

Figure A2. Sensitivity analysis on N_{WG}

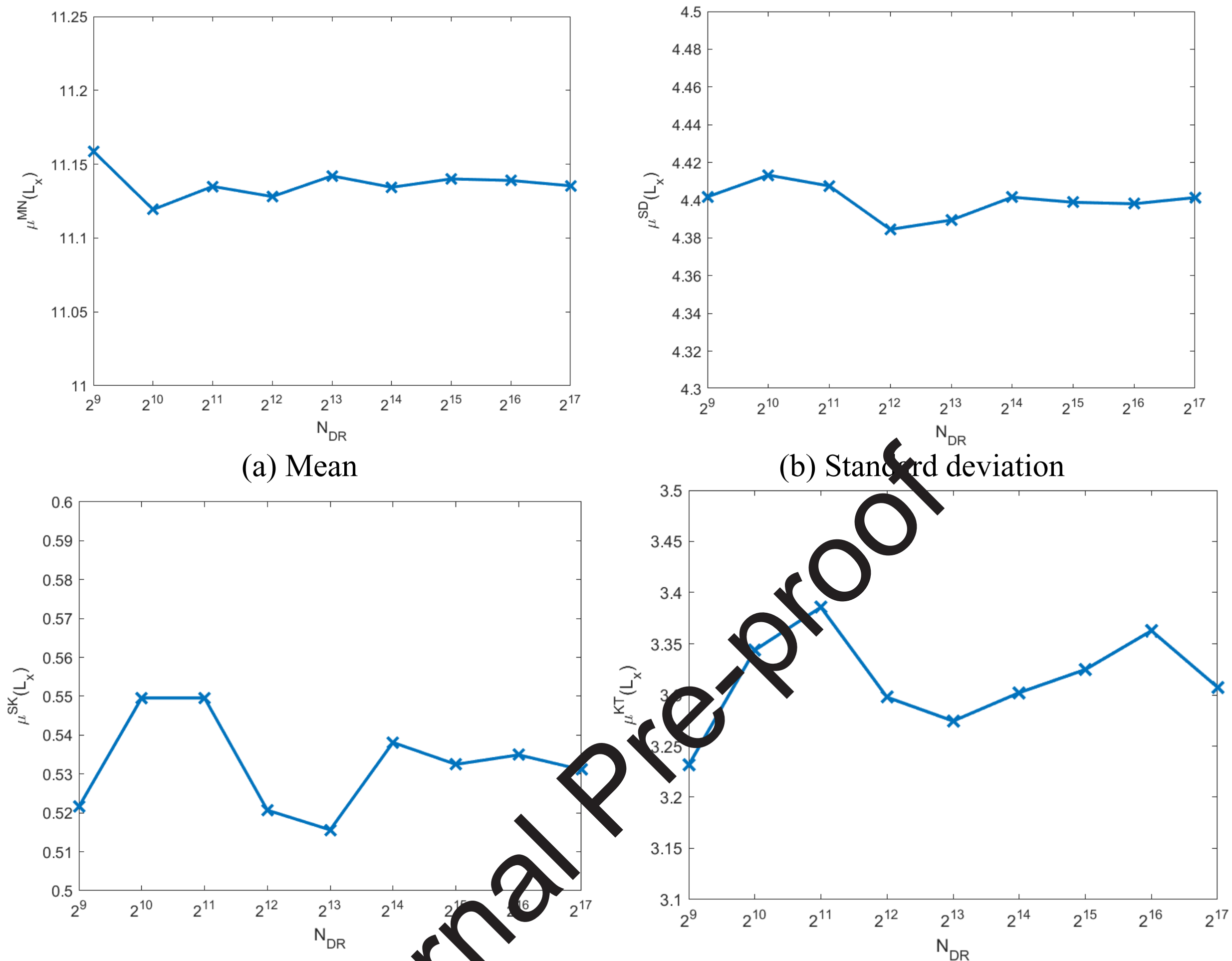

(a) Mean (b) Standard deviation

(c) Skewness (d) Kurtosis

Figure A3. Sensitivity analysis on N_{DR}

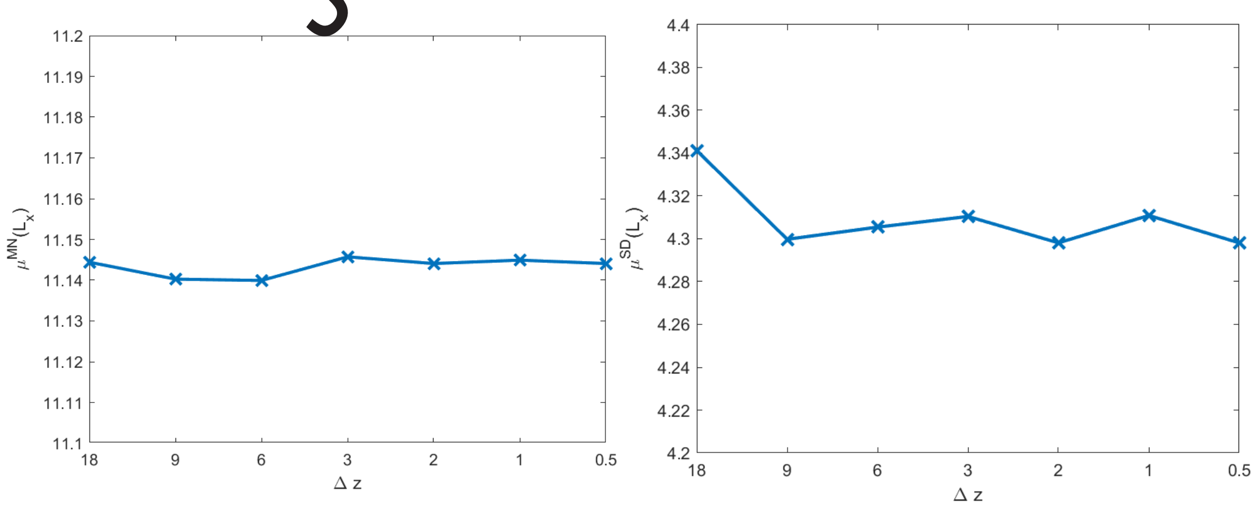

(a) Mean (b) Standard deviation

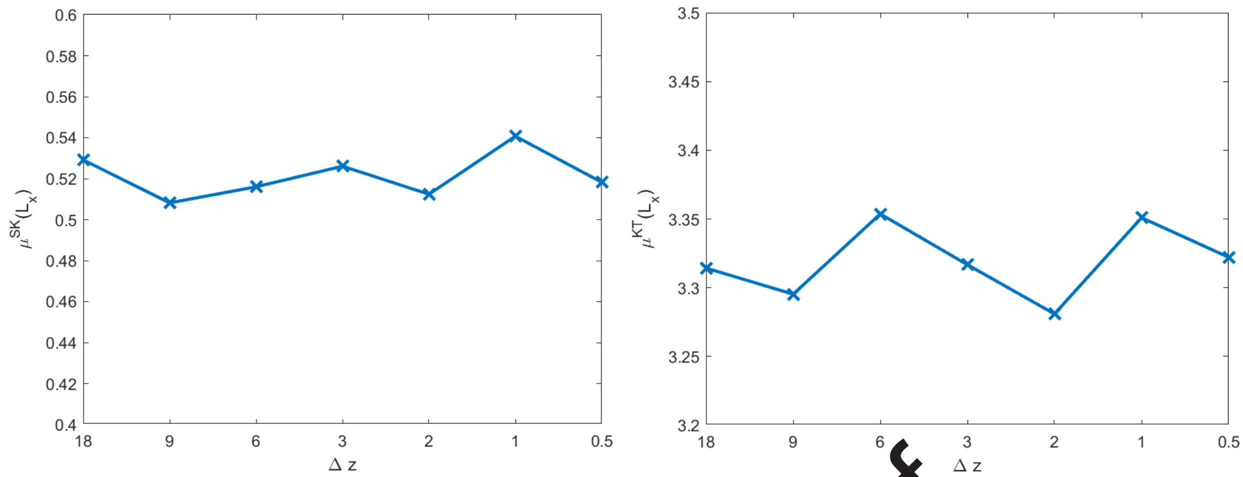

(c) Skewness (d) Kurtosis

Figure A4. Sensitivity analysis on Δz

APPENDIX B: NON-GAUSSIAN WIND SIMULATION BASED ON HERMITE MODEL

The target high-order statistics of skewness and kurtosis are specified respectively as μ_k^{SK} and μ_k^{KT} for different spatial locations *k* (with *k* = 1, 2, …*n*). The corresponding Hermite parameters c_k and d_k can be determined by solving a set of nonlinear equations so that these high-order moments will be matched after translation (Gurley et al., 1997):

$$\mu_k^{SK} = {E_k}^3(8{c_k}^3 + 108c_k{d_k}^2 + 36c_kd_k + 6c_k) \quad \text{(B-1a)}$$

$$\mu_k^{KT} = {E_k}^4(60{c_k}^4 + 3348{d_k}^4 + 2232{c_k}^2{d_k}^2 + 60{c_k}^2 + 252{d_k}^2 + 1296{d_k}^3 + 576{c_k}^2d_k + 24d_k + 3) \quad \text{(B-1b)}$$

with $E_k = \frac{1}{\sqrt{1+2{c_k}^2+6{d_k}^2}}$. Eq. (B-1) can be solved numerically or via close form approximations (Yang et at., 2013). On the other hand, the target PSDM of the non-Gaussian wind fluctuation is prescribed as $\boldsymbol{S}^{\boldsymbol{N}}(\omega)$, where each element $S_{jk}^N(\omega)$ (with *j* and *k* = 1, 2, …*n*) is obtained using the same method as in Eq. (11)-(13) for effective comparison with the Gaussian counterpart (i.e., vary skewness and kurtosis, while keeping PSDM unchanged). Without loss of generality, each term is normalized as:

$$S_{jk}^{N}(\omega)=\frac{S_{jk}^{N}(\omega)}{\sqrt{\int_{-\infty}^{\infty}S_{jj}^{N}(\omega)\mathrm{d}\omega\int_{-\infty}^{\infty}S_{kk}^{N}(\omega)\mathrm{d}\omega}} \quad \text{(B-2)}$$

Based on the target PSDM $\boldsymbol{S^N}(\omega)$, each element $\rho_{jk}^{N}(\tau)$ in the equivalent correlation coefficient function matrix (CCFM) $\boldsymbol{\rho^N}(\tau)$ can be obtained by the inverse Winener-Khintchine relationship:

$$\rho_{jk}^{N}(\tau)=\int_{-\infty}^{\infty}S_{jk}^{N}(\omega)e^{I\omega\tau}\mathrm{d}\omega \quad \text{(B-3)}$$

where I is the imaginary unit. The corresponding correlation coefficient function for the underlying Gaussian process can be obtained via the explicit correlation distortion function (Yang and Gurley, 2015):

$$\rho_{jk}^{G}(\tau)=B-\frac{A}{B}-\frac{c_jc_k}{9d_jd_k} \quad \text{(B-4a)}$$

with

$$A=\frac{1}{18d_jd_k}-\frac{{c_j}^2{c_k}^2}{81{d_j}^2{d_k}^2} \quad \text{(B-4b)}$$

$$B=$$

$$\left[\frac{\rho_{jk}^{G}(\tau)}{12d_jd_kE_jE_k}+\frac{c_jc_k}{108{d_j}^2{d_k}^2}-\frac{{c_j}^3{c_k}^3}{729{d_j}^3{d_k}^3}+\sqrt{\left(\frac{\rho_{jk}^{G}(\tau)}{12d_jd_kE_jE_k}+\frac{c_jc_k}{108{d_j}^2{d_k}^2}-\frac{{c_j}^3{c_k}^3}{729{d_j}^3{d_k}^3}\right)^2+A^3}\right]^{1/3} \quad \text{(B-4c)}$$

The corresponding spectral term $S_{jk}^{G}(\omega)$ in the PSDM for the underlying Gaussian process $\boldsymbol{S^G}(\omega)$ can be then obtained by the Winener-Khintchine relationship:

$$S_{jk}^{G}(\omega)=\frac{1}{2\pi}\int_{-\infty}^{\infty}\rho_{jk}^{G}(\tau)e^{-I\omega\tau}\mathrm{d}\tau \quad \text{(B-5)}$$

With the obtained $\boldsymbol{S^G}(\omega)$, the spatially correlated Gaussian wind fluctuations $u_k^G(t)$ can be conveniently simulated for different locations using the SRM (e.g., Deodatis, 1996). The non-Gaussian wind fluctuations can then be obtained by the third order Hermite functional transformation with previously calculated parameters:

$$u_k^N(t)=E_k\left\{u_k^G(t)+c_k\left[{u_k^G}^2(t)-1\right]+d_k\left[{u_k^G}^3(t)-3u_k^G(t)\right]\right\} \quad \text{(B-6)}$$

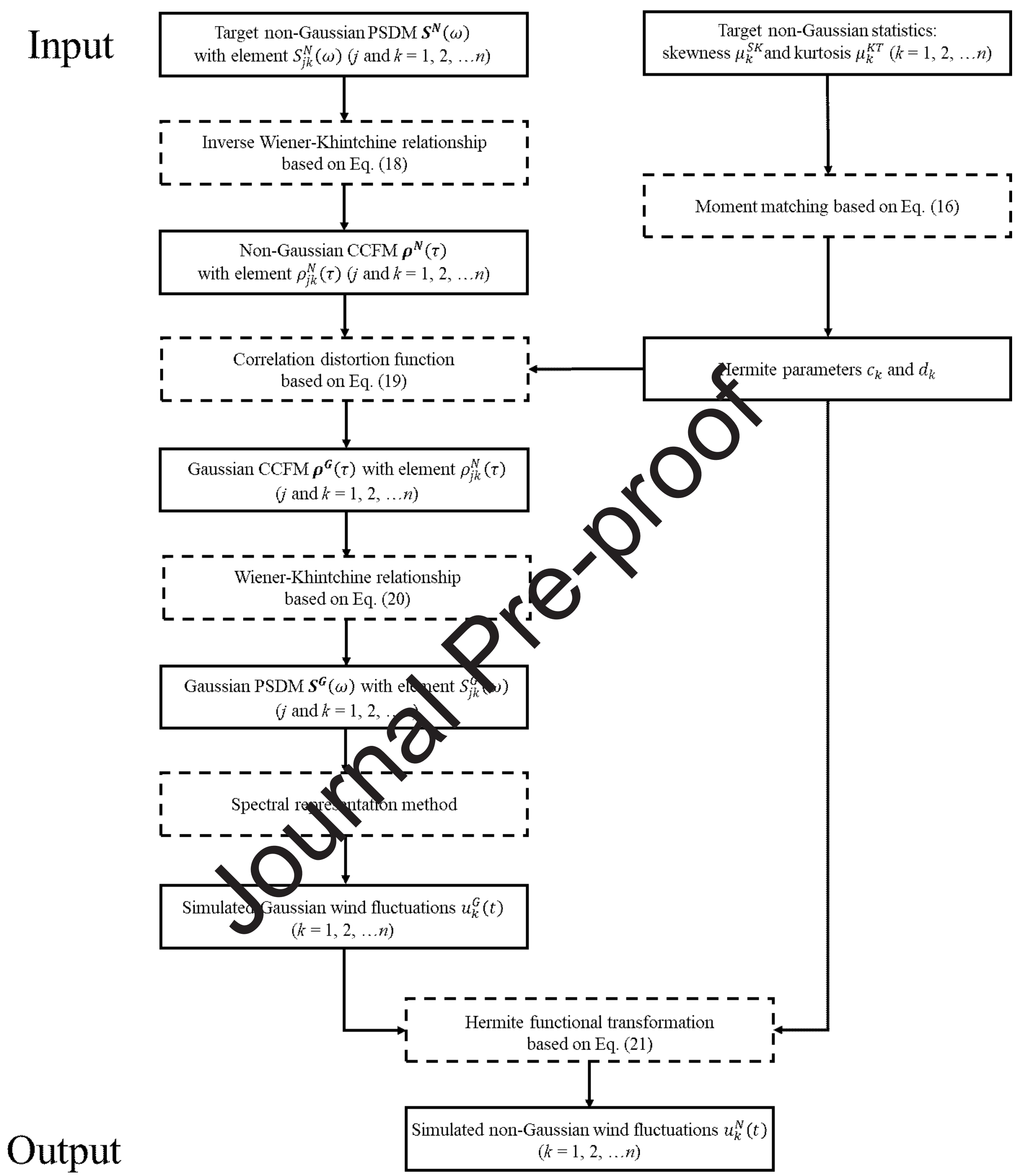

Figure B1. Schematic description of simulating non-Gaussian wind fluctuations based on Hermine model

APPENDIX C: FURTHER INVESTIGATION ON INITIAL-STAGE AND LATER-STAGE TURBULENCE

It is straightforward in Fig. 13 to select the "spatial" half to partition the initial and later stage of debris flight, considering the focus of this study is the effect of "spatial" correlation on debris flight. Noting that debris tend to spend less time on the latter "spatial" half of the flight due to the higher vertical travel speed, it is worthwhile to conduct additional analysis using the "temporal" half with equal travel time for the two stages. The results are shown in Fig. C1. Approximately, the first "temporal" half covers z = 20m to z = 15m, while the second "temporal" half covers z = 15m to z = 0m. The results are similar to that using the "spatial" half in Fig 13, which proves that turbulence at the initial stage of the flight is more critical.

For effective comparison, Fig. C2 depicts 1024 samples of debris flight for the two cases of considering only the initial-stage turbulence and only the later-stage turbulence. As shown in Fig. C2, given the same flight time, the variations in the debris location immediately after the action of turbulence are close for the two cases (the two red boxes). However, even without the action of turbulence in the later stage, the variation in the debris location caused by the turbulence at the initial stage (the red box in the bottom figure) can continue to develop. In this sense, the turbulence effect at the initial stage has twice the "developing" time compared to that of the later-stage turbulence.

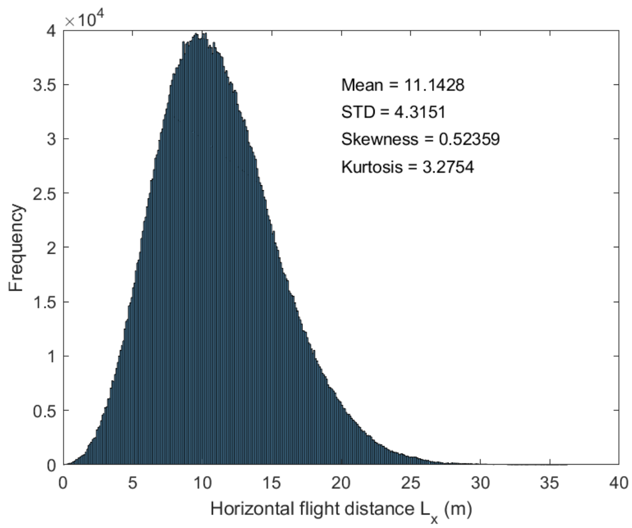

(a) Baseline: repeat of Figure 12(b)

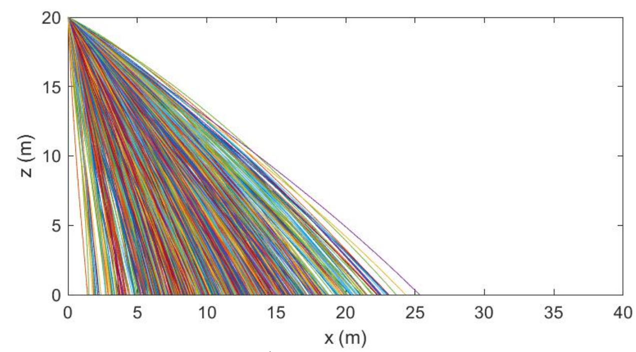

(b) 1024 samples of debris flight trajectories from Fig. C1(a)

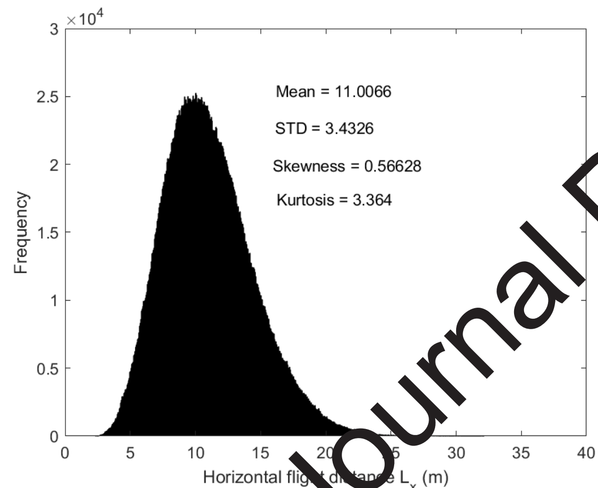

(c) Similar correlation scenario as Fig. C1(a), but no turbulence for debris traveling between z = 15 m and z =0 m (half of the total flight time)

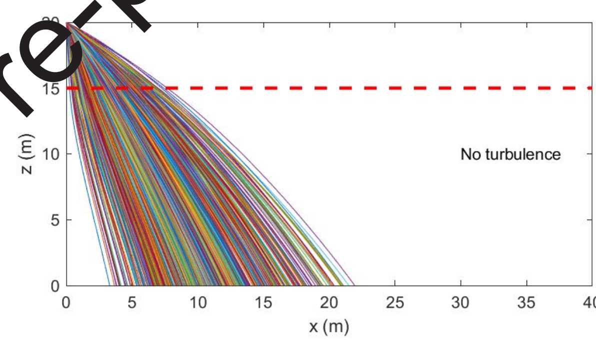

(d) 1024 samples of debris flight trajectories from Fig. C1(c)

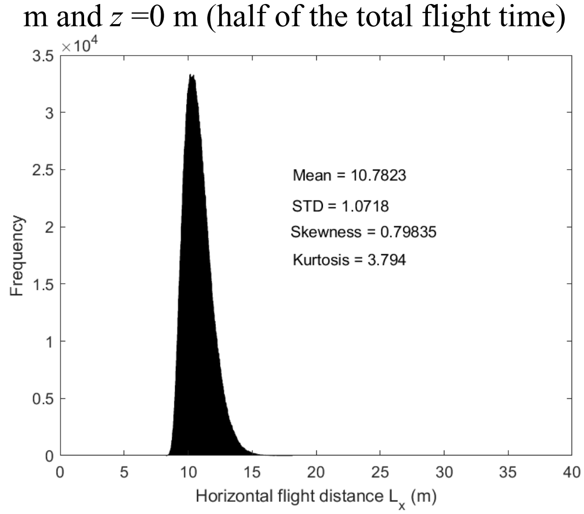

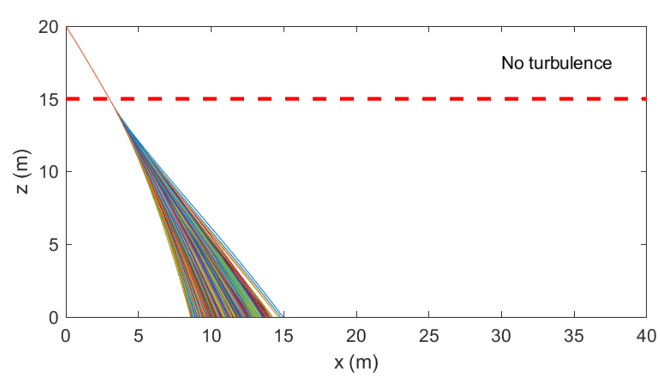

(e) Similar correlation scenario as Fig. C1(a), but no turbulence for debris traveling between z = 20 m to z =15 m (half of the total flight time)

(f) 1024 samples of debris flight trajectories from Fig. C1(e)

Figure C1. Dissection of vertical correlation's influence on debris flight using "temporal" half

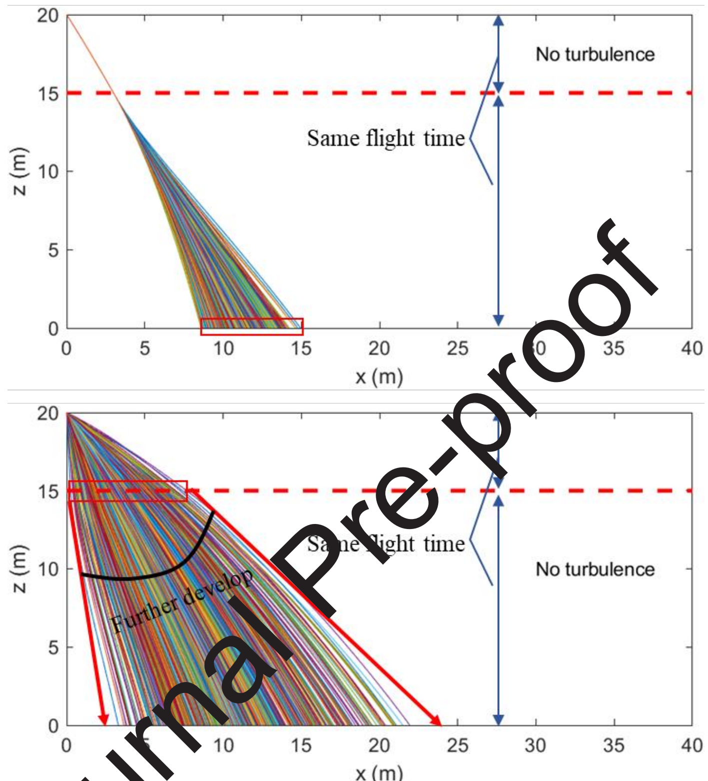

Figure C2. Effect of initial and later-stage turbulence on debris flight

REFERENCES

Abdelhady, A.U., Spence, S.M. and McCormick, J., 2021. A three-dimensional six-degree-of-freedom windborne debris trajectory model for tornadoes. *Journal of Wind Engineering and Industrial Aerodynamics*, 214, 104622.

Ai, X.Q., Lyu, M.Z. and Chen, J.B., 2023. Three-dimensional flight trajectories and impact damage prediction model for wind-borne debris. *Natural Hazards Review*, 24(2), 04023005.

ASCE, 2012, Wind tunnel testing for buildings and other structures, ASCE/SEI 49-12.

ASCE, 2016, Minimum Design Loads and Associated Criteria for Buildings and Other Structures, ASCE/SEI 7-16.

Baker, C.J., 2007. The debris flight equations. *Journal of Wind Engineering and Industrial Aerodynamics*, 95(5), 329-353.

Baker, C.J. and Sterling, M., 2017. Modelling wind fields and debris flight in tornadoes. *Journal of Wind Engineering and Industrial Aerodynamics*, 168, 312-321.

Balderrama, J.A., Masters, F.J. and Gurley, K.R., 2012. Peak factor estimation in hurricane surface winds. *Journal of wind engineering and industrial aerodynamics*, 102, 1-13.

Benowitz, B.A. and Deodatis, G., 2015. Simulation of wind velocities on long span structures: A novel stochastic wave based model. *Journal of Wind Engineering and Industrial Aerodynamics*, 147, 154-163.

Catarelli, R.A., Fernández-Cabán, P.L., Phillips, B.M., Bridge, J.A., Masters, F.J., Gurley, K.R. and Prevatt, D.O., 2020. Automation and new capabilities in the university of Florida NHERI Boundary Layer Wind Tunnel. *Frontiers in Built Environment*, 6, 558151.

Davenport, A.G., 1961. The spectrum of horizontal gustiness near the ground in high winds. *Quarterly Journal of the Royal Meteorological Society*, 87(372), 194-211.

Deodatis, G., 1996. Simulation of ergodic multivariate stochastic processes. *Journal of engineering mechanics*, 122(8), 778-787.

Dong, Y., Guo, Y. and van de Lindt, J.W., 2023. Fragility Modeling of Urban Building Envelopes Subjected to Windborne Debris Hazards. *Journal of Structural Engineering*, 149(5), 04023041.

Dyrbye, C. and Hansen, S.O., 1996. Wind loads on structures.

Fernández-Cabán, P.L. and Masters, F.J., 2017. Near surface wind longitudinal velocity positively skews with increasing aerodynamic roughness length. *Journal of Wind Engineering and Industrial Aerodynamics*, 169, 94-105.

Fernandez, G., Masters, F. and Gurley, K., 2010. Performance of Hurricane Shutters Under Impact by Roof Tiles. *Engineering Structures*, 32(10), 3384-3393.

Grigoriu, M., 1984. Crossings of non-Gaussian translation processes. *Journal of Engineering Mechanics*, 110(4), 610-620.

Grigoriu, M., 1998. Simulation of stationary non-Gaussian translation processes. *Journal of Engineering Mechanics*, 124(2), 121-126.

Gurley, K. and Masters, F., 2011. Post 2004 hurricane field survey of residential building performance. *Natural Hazards Review*, 12(4), 177-183.

Gurley, K., Masters F., Reinhold T., and Ojeda-Tuz, M., 2021. Florida Coastal Monitoring Program Hurricanes Report (1999-2008) in *FCMP Ground Level Hurricane Wind Data (1999-2008)*. DesignSafe-CI. https://doi.org/10.17603/ds2-j82e-nc21

Gurley, K.R., Tognarelli, M.A. and Kareem, A., 1997. Analysis and simulation tools for wind engineering. *Probabilistic Engineering Mechanics*, 12(1), 9-31.

Jain, A., 2015. Hurricane wind-generated debris impact damage to the glazing of a high-rise building. *Forensic Engineering*, 2015, 361-370.

Kakimpa, B., Hargreaves, D.M. and Owen, J.S., 2011, July. A numerical investigation of the influence of launch conditions on windborne debris flight. In *13th international conference on wind engineering (ICWE13)*. Amsterdam, Netherlands.

Karimpour, A. and Kaye, N.B., 2012. On the stochastic nature of compact debris flight. *Journal of wind engineering and industrial aerodynamics*, 100(1), 77-90.

Kordi, B. and Kopp, G.A., 2011. Effects of initial conditions on the flight of windborne plate debris. *Journal of Wind Engineering and Industrial Aerodynamics*, 99(5), 601-614.

He, J.Y., He, Y.C., Li, Q.S., Chan, P.W., Zhang, L., Yang, H.L. and Li, L., 2020. Observational study of wind characteristics, wind speed and turbulence profiles during Super Typhoon Mangkhut. *Journal of Wind Engineering and Industrial Aerodynamics*, 206, 104362.

Holmes, J.D., 2004. Trajectories of spheres in strong winds with application to wind-borne debris. *Journal of Wind Engineering and Industrial Aerodynamics*, 92(1), 9-22.

Hui, M.C.H., Larsen, A.X.H.F. and Xiang, H.F., 2009. Wind turbulence characteristics study at the Stonecutters Bridge site: Part I—Mean wind and turbulence intensities. *Journal of Wind Engineering and Industrial Aerodynamics*, 97(1), 22-36.

Huo, S., Hemida, H. and Sterling, M., 2020. Numerical study of debris flight in a tornado-like vortex. *Journal of Fluids and Structures*, 99, 103134.

Johnson, T., Pinelli, J.P., Baheru, T., Chowdhury, A., Weekes, J., and Gurley, K. 2018. Simulation of rain penetration in buildings and associated damage within a hurricane vulnerability model. *Natural Hazards Review*, 19(2), 04018004.

Li, S., Snaiki, R. and Wu, T., 2021. Active simulation of transient wind field in a multiple-fan wind tunnel via deep reinforcement learning. *Journal of Engineering Mechanics*, 147(9), 04021056.

Lin, N., Letchford, C. and Holmes, J., 2006. Investigation of plate-type windborne debris. Part I. Experiments in wind tunnel and full scale. *Journal of Wind Engineering and Industrial Aerodynamics*, 94(2), 51-76.

Liu, Z., Cao, Y., Wang, Y., Cao, J., Hua, X. and Cao, S., 2021a. Characteristics of compact debris induced by a tornado studied using large eddy simulations. *Journal of Wind Engineering and Industrial Aerodynamics*, 208, 104422.

Liu, Z., Cao, Y., Yan, B., Hua, X., Zhu, Z. and Cao, S., 2021b. Numerical study of compact debris in tornadoes at different stages using large eddy simulations. *Journal of Wind Engineering and Industrial Aerodynamics*, 210, 104530.

Liu, Z., Cao, Y., Wang, Y., Cao, S. and Yang, Q., 2021c. Study of turbulence effects on flying compact debris in tornadoes at different stages. *Journal of Wind Engineering and Industrial Aerodynamics*, 218, 104777.

Liu, Y., Wang, H., Xu, Z., Li, J., Wu, T. and Mao, J., 2023. Modeling Multidimensional Multivariate Turbulent Wind Fields Using a Correlated Turbulence Wave Number–Frequency Spectral Representation Method. *Journal of Engineering Mechanics*, 149(4), 04023010.

Lyu, M.Z., Ai, X.Q., Sun, T.T. and Chen, J.B., 2023. Fragility analysis of curtain walls based on wind-borne debris considering wind environment. *Probabilistic Engineering Mechanics*, 71, 103397.

Maruyama, T., 2011. Simulation of flying debris using a numerically generated tornado-like vortex. *Journal of Wind Engineering and Industrial Aerodynamics*, 99(4), 249-256.

Masters, F.J., Gurley, K.R., Shah, N. and Fernandez, G., 2010. The vulnerability of residential window glass to lightweight windborne debris. *Engineering Structures*, 32(4), 911-921.

Minor, J.E., 1994. Windborne debris and the building envelope. *Journal of Wind Engineering and Industrial Aerodynamics*, 53(1-2), 207-227.

Moghim, F. and Caracoglia, L., 2012a. A numerical model for wind-borne compact debris trajectory estimation: Part 1–Probabilistic analysis of trajectory in the proximity of tall buildings. *Engineering Structures*, 38, 153-162.

Moghim, F. and Caracoglia, L., 2012b. A numerical model for wind-borne compact debris trajectory estimation: Part 2–Simulated vertical gust effects on trajectory and mass momentum. *Engineering Structures*, 38, 163-170.

Moghim, F. and Caracoglia, L., 2014. Effect of computer-generated turbulent wind field on trajectory of compact debris: A probabilistic analysis approach. *Engineering structures*, 59, 195-209.

Moghim, F., Xia, F.T. and Caracoglia, L., 2015. Experimental analysis of a stochastic model for estimating wind-borne compact debris trajectory in turbulent winds. *Journal of Fluids and Structures*, 54, 900-924.

Ojeda-Tuz, M., Gurley K., Shields M., Chauhan M., Catarelli R. and Masters F., 2023, Wind Profiles in a Boundary Layer Wind Tunnel based on Different Approach Terrain Configurations in *Modeling of Higher-Order Turbulence from Randomize Terrain in a Boundary Layer Wind Tunnel*. DesignSafe-CI. https://doi.org/10.17603/ds2-h4pt-d221 v1

Pita, G., Pinelli, J.P., Gurley, K., Weekes, J., Cocke, S., and Hamid, S., 2016. Hurricane vulnerability model for mid/high-rise residential buildings. *Wind and Structures*, 23(5), 449-464.

Taylor, G.I., 1938. The spectrum of turbulence. *Proceedings of the Royal Society of London. Series A-Mathematical and Physical Sciences*, 164(919), 476-490.

Wei, Z., Pinelli, J.P. and Gurley, K., 2024a. Component-Based Hurricane Vulnerability Model for Mid/High-Rise Commercial Residential Buildings. *International Journal of Disaster Risk Reduction,* 100, 104222.

Wei, Z., Pinelli, J.P., Gurley, K., Hamid, S. and Flannery, G., 2024b. Component-Based Estimation of Recovery Time and Time-Related Expenses after Hurricane Events. *Frontiers in Built Environment*, 9, 1295619.

Yang, L., Gurley, K.R. and Prevatt, D.O., 2013. Probabilistic modeling of wind pressure on low-rise buildings. *Journal of Wind Engineering and Industrial Aerodynamics*, 114, 18-26.

Yang, L. and Gurley, K.R., 2015. Efficient stationary multivariate non-Gaussian simulation based on a Hermite PDF model. *Probabilistic Engineering Mechanics*, 42, 31-41.

Zhang, X., Hao, H. and Ma, G., 2013. Laboratory test and numerical simulation of laminated glass window vulnerability to debris impact. *International Journal of Impact Engineering*, 55, 49-62.

Zhao, L., Cui, W. and Ge, Y., 2019. Measurement, modeling and simulation of wind turbulence in typhoon outer region. *Journal of Wind Engineering and Industrial Aerodynamics*, 195, 104021.

Zhao, J., Yan, G. and Han, D., 2021. A review of approaches to simulate windborne debris dynamics in wind fields. *Journal of Wind Engineering and Industrial Aerodynamics*, 212, 104597.

Declaration of interests

☒ The authors declare that they have no known competing financial interests or personal relationships that could have appeared to influence the work reported in this paper.

☐ The authors declare the following financial interests/personal relationships which may be considered as potential competing interests: